Electrical Power and Energy Systems 156 (2024) 109737

Contents lists available at ScienceDirect

International Journal of Electrical Power and Energy Systems

journal homepage: www.elsevier.com/locate/ijepes

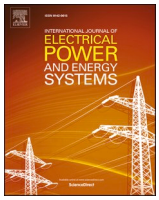

Integration of wind and solar energies with battery energy storage systems into 36-zone Great Britain power system for frequency regulation studies

Rasoul Azizipanah-Abarghooee [a], Mostafa Malekpour [a,*], Mazaher Karimi [b,*], Vladimir Terzija [c]

[a] Energy Advisory Department, WSP, Manchester, UK
[b] School of Technology and Innovations, University of Vaasa, Vaasa, Finland
[c] School of Engineering, Merz Court E4.41, Newcastle University, UK

ARTICLE INFO

Keywords:
Benchmark
36-zone Great Britain power system
Droop-based frequency response
Inertial power
Rate of change of frequency

ABSTRACT

Variable-speed wind generators (VSWGs) and solar Photovoltaic (PV) units are being broadly employed as the main renewable energy sources in large-scale transmission power networks. However, they can cause system stability challenges following power imbalances since they provide no inertial and governor responses. In this study, generic dynamic models are developed for VSWGs, PVs and battery energy storages systems (BESSs) which include inertia emulator and droop-based frequency control schemes. These models are suitable for transmission systems stability studies and are integrated into 36-zone Great Britain (GB) power system in DIgSILENT PowerFactory. It is a very useful benchmark for academic research and industrial sectors to undertake feasibility studies for renewable energy integration into GB power system. However, it is not an exact equivalent of the real GB power system. The dynamic time-domain simulations and modal analysis are provided and justified to investigate how PV, Wind and BESS units affect the system frequency response. A sensitivity analysis is also carried out against several factors to demonstrate the dynamic performance of the test system incorporating the generic models for VSWGs, PVs and BESSs. These are associated with units' frequency response and system frequency changes under renewable energies' penetration levels of 20 %, 25 %, 50 %, 60 % and 75 % of system demand.

1 Introduction

Frequency control of power systems has become considerably a challenging task for network operators due to nowadays large-scale integration of renewable energy sources (RESs) like wind/photovoltaic power into electricity systems like Denmark, Germany, and UK. To investigate and tackle the issues like growing frequency nadir, rate of change of frequency (RoCoF) and steady-state frequency deviation, the operation guidelines of grid codes need to be revisited and power system network benchmark should consider high integration of RESs in a way that RESs can take part in system frequency maintenance. In the UK, there are three frequency mechanisms comprising of firm frequency response, mandatory frequency response and frequency control by demand management. WTs and PVs should have primary frequency control by deploying the stored kinetic energy (inertial emulator) of wind energy conversion systems (WECSs) or energy stored in dc link capacitor of PVs or de-loaded maximum power point tracking (MPPT) for both WECSs and PVs to regulate their output following the frequency excursion [1].

The contribution of RESs to the system frequency regulation becomes a topic of interest in the area. For instance, the inertial emulator and droop controllers are presented in [2-6] for WECS, while identical methods can be found in [7] for battery energy storage system (BESS) and PV-BESS [8,9]. In the case of inertial emulator of WECS, it operates in the classical MPPT mode and releases inertial energy stored in the wind turbine (WT) shaft [10,11]. However, in droop-based frequency regulation strategy, WECS operates in a de-loaded situation obtained by either operating at the suboptimal rotor speed [12] or pitching the angle of blade [13] to deliberately employ spill power and reserve energy for the primary frequency response. Furthermore, other converter-based sources like PVs do not naturally have a stored energy source to provide the emulated inertial response while sufficient energy is stored in their power converter systems [14]. In addition, there are several methodologies that integrate the frequency supports from RESs into operational planning scheme to coordinate discrepant frequency responses and meet frequency control requirements [15-17]. However, all

* Corresponding author.
E-mail address: mazaher.karimi@uwasa.fi (M. Karimi).

https://doi.org/10.1016/j.ijepes.2023.109737
Received 30 August 2023; Received in revised form 6 November 2023; Accepted 20 December 2023

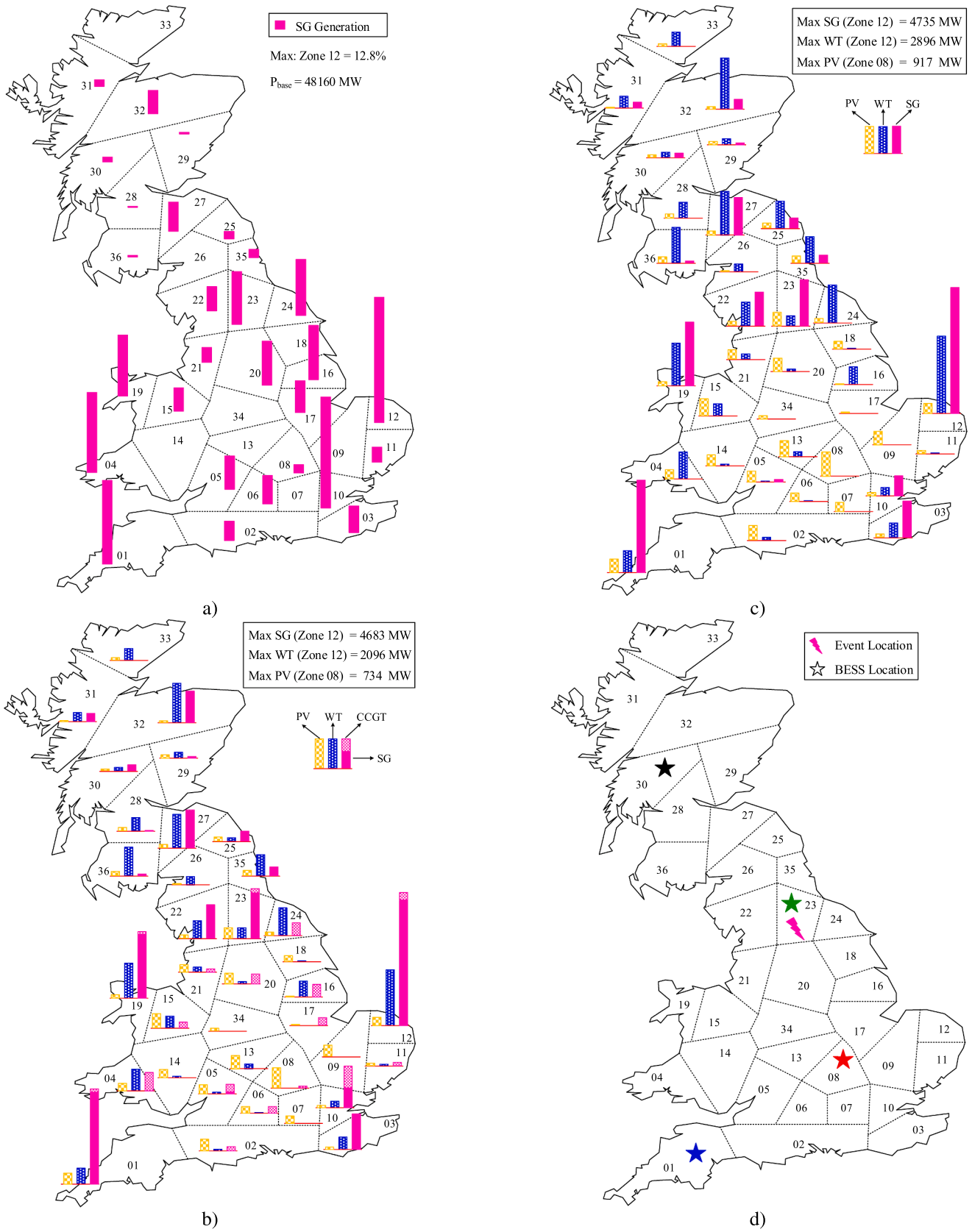

Fig. 1. Geographic distribution of (a) SG generation in "WTPV 00 %" scenario; and (b) Geographic distribution of power plant's generations in "WTPV 60 %" scenario; (c) Geographic distribution of power plant's generations in "WTPV 75 %" scenario and d) Loss of generation event location and BESSs installation locations.

the state-of-the-art approaches have some drawbacks that need further investigations. For instance, droop based suboptimal rotor speed is limited by rotor speed and suffered by wind speed measurement errors [18]. When they cannot be put in place, an interesting alternative like deploying BESSs should be investigated.

In order to reach the above noticed goal in practical cases, UK National Grid have been investigating different ways to tackle these challenges caused by the variability and uncertainty of wind speed and solar irradiance and find out how a WT and PV can provide a reliable frequency response. BESSs are optimally suitable to meet the incipient challenge due to its fast response and high ramp rate [19]. Primary frequency support is found to be the most beneficial service by BESSs in the Danish network [20] and Li-ion BESSs can fulfil this ancillary service. BESSs installations will go beyond 65GWh in UK in 2030 [21]. The frequency response of UK power systems might be significantly enhanced by electric vehicle based BESSs [22], however, a large number of electric vehicles can potentially put the system frequency stability at risk [23]. A BESSs is deployed in [24] as an effective regulation source to instantaneously respond to the frequency excursion. It is notable that the widespread BESS employment is restricted by high capital costs.

In the current literature, the droop and inertial response impact of WECSs, PVs and BESSs on a large-scale practical test system are completely ignored. A reduced 39-bus power grid [25], a single-bus small-scale power grid system [26], a simple single-bus simulation system [27], a typical small-scale Northern Ontario, Canada-based rural distribution system [28], a simple two-bus test system [29], a simplified system frequency response [30], two-area Kundur model and IEEE 39-bus system [31], and a ten bus system [32] are implemented to show only the impact of WECSs on small test systems. Moreover, there exist several power networks where researchers are forced to choose their own dynamic modelling and parameters that lead to contradiction [33]. This paper derives a real-world, empirically grounded and well-organized 50 Hz 36-zone GB system model as endorsed by National Grid (NG) of UK for frequency control-based benchmark system and presented in [34]. The dynamic parameters for a sixth order and fifth order cylindrical round and salient pole rotors synchronous machine models comprising of 41 power stations of low (20 %, 25 %) and medium (50 %, 60 %) RESs penetration, 22 gas turbines including of combined cycle gas turbine (CCGT), 6 nuclear power stations, 8 biomass plants, 4 hydroelectric generations and 1 pumped storage unit, voltage controllers (VCOs), power system stabilizer (PSSs) and governors (GOVs) are considered. Additionally, variable speed wind generators (VSWGs) penetrations tend to be large, and thus, the size of the largest in-feed has increased, major frequency excursions may become more probable, and the influence on the system should be analysed. Whereas the developed benchmark model is configured using basic features and data from UK NG and applied in DIgSILENT PowerFactory [35], it can be linked or extended with other software packages. Consequently, the users of this test system can straightforwardly tune its characteristics to gratify their preferences, or to model and investigate other problems that have not yet been deployed for this grid. As such, this paper demonstrates how to integrate discrepant types of RESs into the 36-zone GB equivalent system which has been deployed by several academic and industrial researchers. Furthermore, this paper presents the technological readiness level of this test system to be deployed for designing industrial applications like feasibility studies for RESs developers. The results with their diverse sensitivity analysis can be used as a good reference particularly for comparison studies. Therefore, the major contributions of this paper are as follows:

- The equivalent GB 36-zone power system as a dynamic benchmark system is proposed for low, medium and high share of renewable generations.
- The frequency control schemes, including droop-based response and inertia emulator, are designed for VSWGs, PVs and BESS systems.
- Accuracy of the dynamic models is validated by simulations on the 36-zone GB power system under various integration levels of renewable energies.
- Sensitivity analysis is conducted under different operating conditions, to assess impact of the key parameters on the system frequency response.

The 36-zone GB power system model differs in purpose and scale from previously derived power systems. Moreover, the effect of the dynamics of WECSs, PVs and BESSs on its frequency deviations is studies. The effectiveness of the developed controllers for WECS, PVs and BESSs in terms of stability and frequency regulation enhancement is also evaluated. Time-domain simulation results are presented to verify the analytical analysis and discussions like frequency, rate of change of frequency (RoCoF), inertial power change, turbine power change, wind turbine (WT) speed variation, pitch angle, tip speed ratio, power coefficient, torque, location of pre- and post-event operating points of wind turbines on maximum power point tracking (MPPT) characteristics in power coefficient versus pitch angle and tip speed ratio and MPPT turbine power versus pitch angle and MPPT turbine speed, inertial power order changes, up rate limits of inertial power order, influence of wind speed and inertial power on the aforesaid variables and dc link voltage level in low (20 %, 25 %) and medium (50 %, 60 %) wind penetration levels. Furthermore, the inertial response and droop-based frequency. In addition, high integration of RESs' impacts on frequency response of the system is investigated under a case with 75 % penetration rate. The developed model is a practical benchmark model utilized in enhanced frequency control capability (EFCC) project [36,37] and several work packages of MIGRATE project [38] in collaboration with industry and university partners like Alstom or General Electric (GE), Belectric, Centrica, Flexitricity, University of Manchester, University of Strathclyde, Delft University of Technology, and Centro de Investigación de Recursos y Consumos Energéticos Universidad de Zaragoza.

This paper is organized as follows: Section 2 outlines the modelling of all components especially WECSs, PVs, and BESSs in DIgSILENT PowerFactory. The influence of these devices' frequency response is presented in Section 3 and 4 which conveys many interesting characteristics of the WECS, PV, and BESSs in large-scale 36-zone GB network. Finally, Section 5 summarizes the conclusions.

2. Great Britain 36-Zone power system with high integration of RESs

In this section, a general description of the proposed 36-zone test system with high integration of RESs is first provided. Afterwards, the developed approach for power stations modeling is presented.

2.1. The test system description

The single line diagram of the 36-zone test system is depicted in Fig. 1 (a) where the zones are connected to each other's using 69 transmission lines at 400 kV voltage level. In each zone, the synchronous generators are connected to the zone 400 kV terminal through 33 kV/400 kV two-winding transformers with 17 % short-circuit voltage. The generation power and geographical distribution of traditional plants are shown in Fig. 1 (a). It is to be noted that almost 90 % of network

Table 1
Active Power of Conventional Power Plants in 5 Discrepant RESs' Penetration Levels.

No.	Type	Zone	WTPV 00 % (MW)	WT 25 % (MW)	WT 50 % (MW)	WTPV 60 % (MW)	WTPV 75 % (MW)
01	Gas	01	809	531	252	140	–
02	Nuclear	01	3337	3343	3468	3436	3474
03	Gas	02	946	620	294	164	–
04	Nuclear	03	1299	1301	1350	1337	1352
05	Gas	04	3941	2585	1226	683	
06	BioMass	05	100	100	100	100	100
07	Gas	05	1575	1033	490	273	–
08	Gas	06	1385	909	431	240	–
09	Gas	08	420	276	131	73	–
10	BioMass	10	741	742	742	742	742
11	Gas	10	4732	3105	1473	820	–
12	Gas	11	751	493	234	130	–
13	Gas	12	1609	1055	501	279	–
14	Nuclear	12	4548	4555	4726	4683	4735
15	Gas	15	1180	774	367	204	–
16	Gas	16	2704	1774	841	469	–
17	Gas	17	1544	1013	481	268	–
18	Gas	19	617	405	192	107	–
19	Nuclear	19	2398	2400	2400	2400	2400
20	Gas	20	2172	1425	676	376	–
21	Gas	21	724	475	225	125	–
22	Nuclear	22	1202	1204	1249	1238	1251
23	BioMass	23	1722	1724	1724	1724	1724
24	Gas	23	858	563	267	149	–
25	Gas	24	2759	1810	859	478	–
26	BioMass	25	366	366	366	366	366
27	BioMass	27	120	120	120	120	120
28	Gas	27	107	70	33	19	–
29	Nuclear	27	1214	1216	1261	1250	1264
30	Gas	28	18	12	6	3	–
31	BioMass	29	52	52	52	52	52
32	Gas	29	14	9	4	2	–
33	Hydro	30	232	233	233	233	158
34	Hydro	31	321	322	322	322	218
35	Gas	32	11	7	3	2	–
36	Hydro	32	535	536	536	536	363
37	Pump Storage	32	611	612	612	612	–
38	BioMass	35	280	280	280	280	280
39	Gas	35	126	83	39	22	–
40	BioMass	36	45	45	45	45	45
41	Hydro	36	33	33	33	33	22
Total Active Power (MW)			48,157	38,209	28,644	38,209	18,666

Table 2
Active power of PV and WT power plants in WTPV 75 % scenario.

Zone	PV (MW)	WT (MW)	Zone	PV (MW)	WT (MW)
01	509	805	19	162	1624
02	539	84	20	520	88
03	114	537	21	346	184
04	334	1003	22	169	880
05	425	45	23	493	366
06	311	24	24	143	1412
07	335	1	25	179	112
08	917	2	26	43	297
09	490	2	27	150	1653
10	123	328	28	170	589
11	119	45	29	141	212
12	380	2896	30	94	186
13	607	183	31	15	455
14	404	57	32	94	1938
15	646	451	33	102	544
16	46	661	34	114	1
17	40	1	35	247	985
18	272	16	36	207	1334
			Total	10,000	20,000

generation is located in the southern part of UK i.e. England & Wales and Scotland supplies only 10 % of whole system load demand. As mentioned, the largest unit is the nuclear power plant located in zone 12, which supplies 13 % of whole system generation. It is to be noticed that 60 % and 30 % of conventional generating units are CCGT and nuclear power plants, respectively. The remaining 10 % generating units include 10 % biomass and 3 % hydro turbine.

In order to analyze the effect of conventional power plants' replacement with PV and WT power plants, three different scenarios of WTPV 00 %, WTPV 60 % and WTPV 75 % are considered. In the first scenario, the whole system load is satisfied by conventional synchronous generators (SGs). In the second scenario, the PVs and WTs supply 20 % and 60 % of GB network demand, respectively. In the third scenario, the PVs and WTs supply 25 % and 50 % of GB network demand, respectively. Since the total load demand of the network is 40 GW, the power generation of PVs and WTs are 8 GW and 16 GW, respectively. The precise generation of SGs, PVs and WTs are tabulated in Tables 1 to 4. As the penetration of renewable energy sources increases, the capacity of gas turbines based CCGT are decreased while other conventional units' capacity is fixed. The capacity of CCGTs is 5 GW and i.e. 12.5 % of load demand in WTPV 60 % scenario. On the other hand, 27.5 % of load is supplied by nuclear, biomass and hydro-turbine power stations in this scenario. The geographical distribution of generated power of all units are shown in Fig. 1 (b) and Fig. 1 (c) for WTPV 60 % and WTPV 75 %, respectively. Furthermore, the CCGT participation in supplying load demand is separately shown. By comparing this figure and Fig. 1 (a), it is clearly observable that the conventional units placed beside the coast i.e. nuclear units and the biomass power plants located in the middle part of GB network are considered while the gas turbine units of middle-down part of GB network, that is, the high-densely consumption region are substituted with PVs. Moreover, in order to supply all deliverable power of gas turbines in the top areas and coasts of network i.e. low-densely consumption region, the WTs are installed and connected to the associated buses. It be seen from Table 1 in the WTPV 75 % scenario that as the penetration of renewable energy sources increases, the gas turbines are removed while other conventional units' capacity is fixed. However, the capacity of pumped storage unit located in zone 32 is zero in WTPV 75 % scenario. The location of events and BESS is illustrated in Fig. 1 (d).

It is to be noted that two more discrepant low and high penetration of just wind units i.e. WT 25 % Scenario and WT 50 % Scenario are considered to investigate the effect of replacement of conventional generating units with WECSs. In these two scenarios, 25 % and 50 % of load demand are supplied by WECSs, respectively. Since total load

Table 3
Active power of PV and WT power plants in WTPV 60 % scenario.

Zone	PV (MW)	WT (MW)	Zone	PV (MW)	WT (MW)
01	407	609	19	129	1312
02	431	61	20	416	95
03	92	459	21	277	198
04	267	824	22	135	641
05	340	49	23	395	394
06	249	26	24	114	1025
07	268	1	25	144	121
08	734	2	26	34	299
09	392	2	27	120	1251
10	98	252	28	136	511
11	95	49	29	113	221
12	304	2096	30	75	138
13	486	197	31	12	335
14	323	61	32	75	1469
15	517	438	33	82	426
16	37	578	34	91	1
17	32	1	35	198	781
18	218	17	36	165	1060
			Total	8000	16,000

Table 4
Active Power of Wind Power Plants in WT 25 % and WT50 %.

Zone	Active Power in WT 25 % Sc. (MW)	Active Power in WT 50 % Sc. (MW)	Zone	Active Power in WT 25 % Sc. (MW)	Active Power in WT 50 % Sc. (MW)
01	**403**	**805**	**19**	**812**	**1624**
02	42	84	20	44	88
03	268	537	21	92	184
04	502	1003	22	440	880
05	23	45	23	183	366
06	12	24	24	706	1412
07	0	1	25	56	112
08	1	2	26	148	297
09	1	2	**27**	**827**	**1653**
10	164	328	28	294	589
11	23	45	29	106	212
12	**1448**	**2896**	30	93	186
13	91	183	31	228	455
14	28	57	**32**	**969**	**1938**
15	226	451	33	272	544
16	331	661	34	1	1
17	0	1	35	492	985
18	8	16	36	667	1334
			Total	10,000	20,000

demand of 36-zone GB network is 40 GW, total power generated by WECSs are 10 GW and 20 GW in two scenarios. The accurate generated power of conventional power plants and WECSs are listed in Tables 1 to 4. As shown, although the combined cycle gas turbines' (CCGTs') power capacity is reduced as a consequence of WECSs' penetration level increment, the capacity of other conventional units is fixed. It is to be noted the power capacity of WECSs is zero in WT 00 % Scenario.

In order to clearly understand how traditional generators are

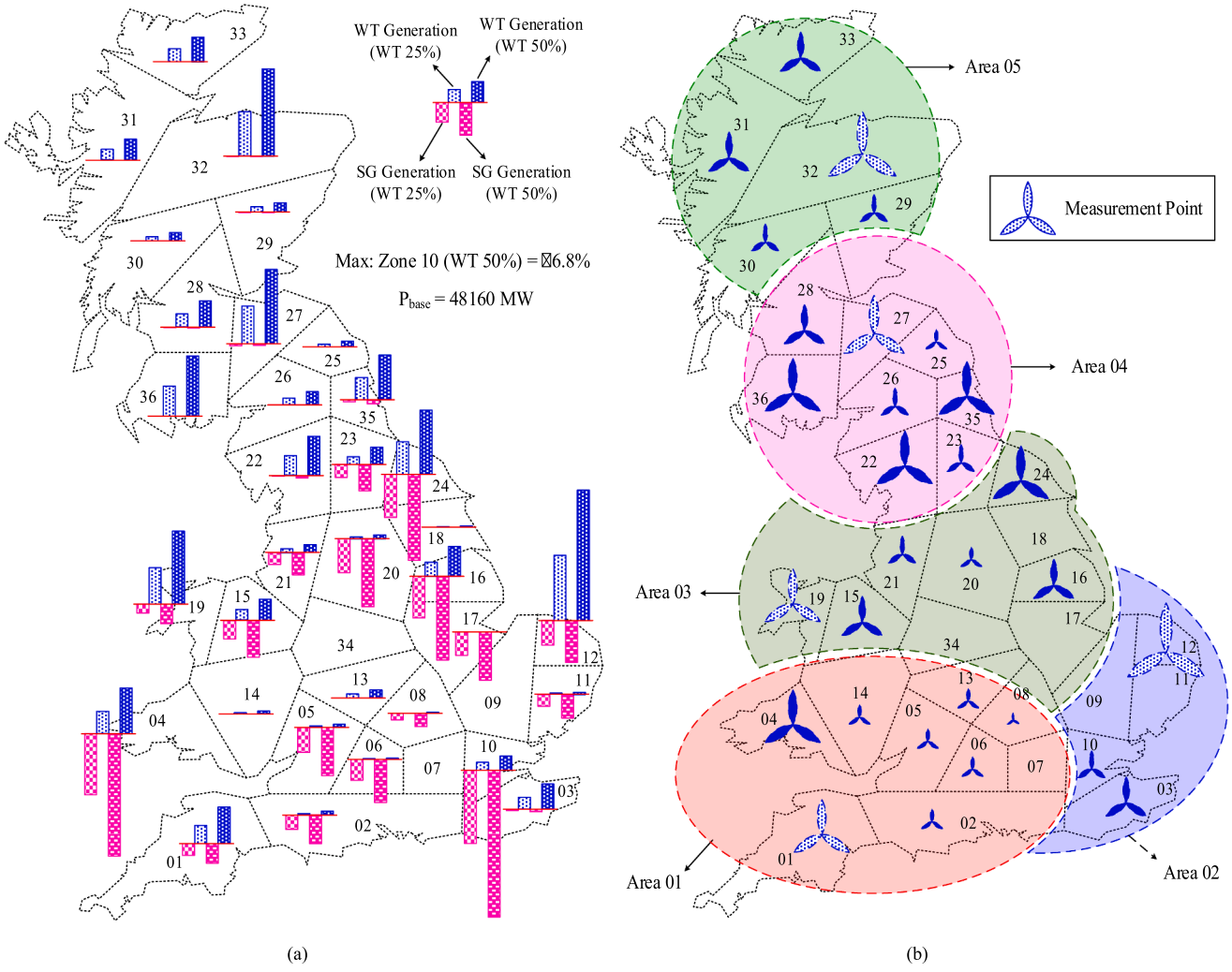

Fig. 2. (a) SG and WT generation deviations in "WT 25 %" and "WT 50 %" scenarios and (b) Area boundaries and measurement points.

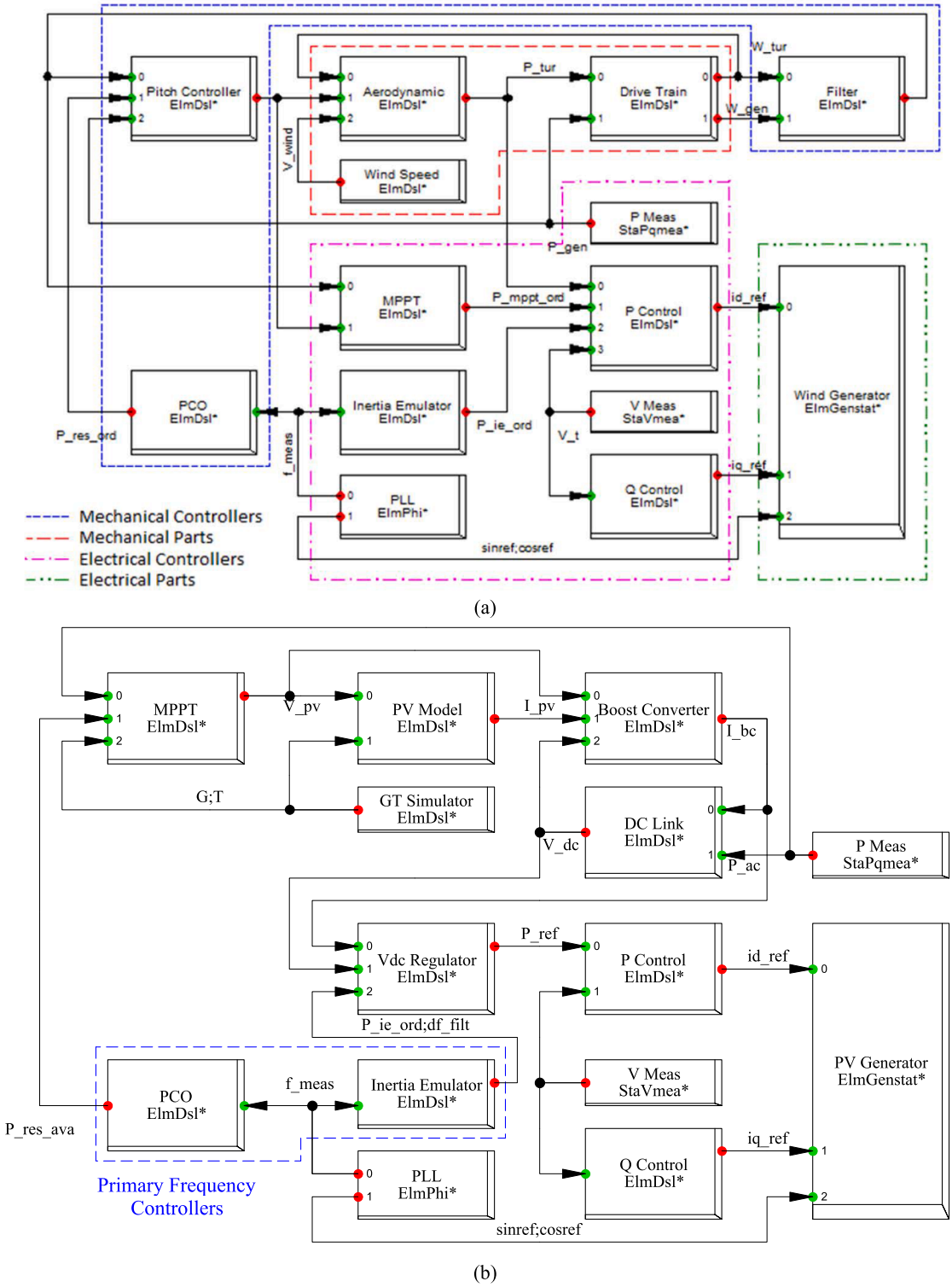

Fig. 3. Control structure of (a) WECS, (b) PV and (c) BESS in DIgSILENT PowerFactory.

substituted with WECSs, the power change of these units for two more scenarios of WT 25 % and WT 50 % with respect to base scenario of WTPV 00 % is portrayed in Fig. 2 (a). It is to be noticed that the maximum variation is related to gas unit located in zone 10 so that its power generation in scenario WT 50 % is dropped down by 70 % compared to base scenario 00 % WT. It can also be deduced that the power generation contribution of northern area is increased with respect to WT 00 % scenario. It means that the replacement procedure is

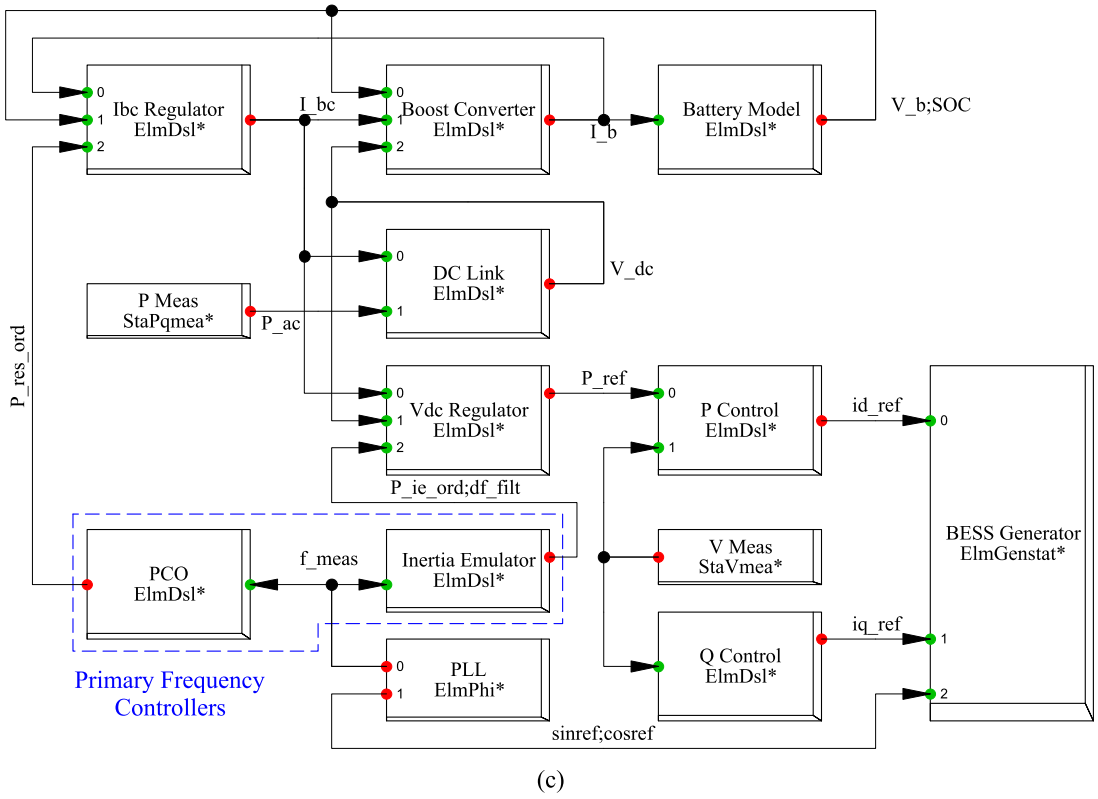

(c)

Fig. 3. (*continued*).

accomplished in a way to balance the geographical distribution of network generation between south and north of 36-zone GB model. In order to monitor and investigate the system frequency response of WECSs alongside conventional units' response, the 36-zone GB network is divided into 5 geographical regions, as shown in Fig. 2 (b). In each region, the frequency response curves and quantities of WECSs highlighted by 'Measurement Point' are tabulated for each incident.

2.2. WECS, PV and BESS models

WECS can be explained as an energy conversion system which can harness the VSWT is shown in Fig. 3 (a). This structure consists of four main modelling parts of mechanical equipment, mechanical controllers, electrical equipment, and electrical controllers. The mechanical parts comprise of blades, turbine shaft, and drive train. Generator, power electronic converters and transformers constitute the electrical part. The mechanical power generated in mechanical part is transferred to the generator via double-mass drive train. The focus of maximum power point tracker (MPPT) is to control the operating point of WT. In VSWT, the injected power to the grid is controlled by power electronic converters using Pref. The reference power Pref is determined by MPPT. One of the most significant advantages of this approach is that it can operate without measuring wind speed. In addition, Fig. 3 (a) shows the whole structure of controlling pitch angle to determine the operating point of VSWT and keep the additional available power as reserve for it. Therefore, the reference pitch angles are determined by the primary controller in proportion of reserve power. Consequently, the pitch controller tunes the pitch angle using servo motors. Finally, the MPPT surface regulates reference power in terms of WT speed and pitch angle. This is a generic and accurate model constructed to be appropriate for dynamic frequency studies in large scale test systems. Additionally, the model considers the physical restrictions of the machine such as pitch angle, power injection and their rates of change. As time interval of 30 s has to be simulated to investigate the WECS model for dynamic frequency studies especially in large scale test systems, the detailed model, which models all the switching procedures results in an overly-long simulation time. Therefore, an average model of the VSWT is deployed, where the electrical generator and power electronic converter is treated as a current source in the proposed WECS. The primary frequency response capability has been integrated into the WECS model [39] and [40].

A generic grid connected two stages PV system with boost stage is deployed and modeled as in Fig. 3 (b) [41]. In this two-stage structure, two power electronic converters in cascade are used to convert the generated power of PV module to AC power. As a result, the DC-DC boost converter increases the voltage of PV modules, and the maximum power can be simultaneously captured by setting the voltage of PV module to MPP [42]. In the next stage, the voltage source inverter converts the DC link voltage to three-phase AC one that can be reached to the network voltage using a transformer. In practice, an LCL filter that is effective in the reduction of switching frequency harmonics is located between the inverter's output side and transformer. Since a short-time simulation must be considered to investigate the PV model for dynamic frequency studies especially in large scale test systems, the detailed model, which

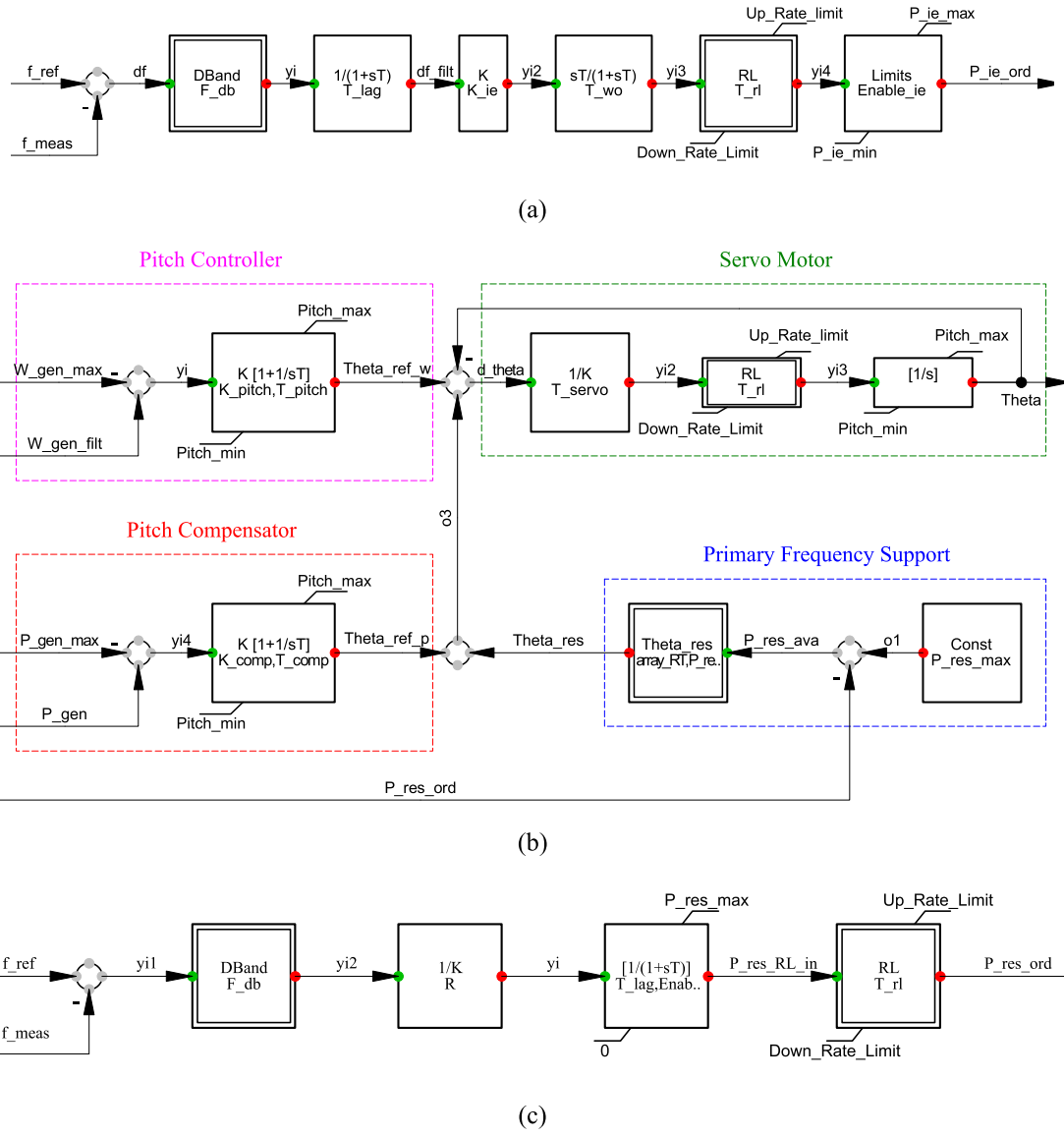

Fig. 4. (a) Outline of WECS Inertia Emulator (b) Outline of WECS pitch controller, (c) Outline of WECS primary controller (PCO).

Table 5
Pitch Controller Parameters.

Parameter	Value	Parameter	Value
$W_{gen,max}$	1.1p.u.	$P_{gen,max}$	1.2
K_{pitch}	38.6 deg/p.u.	T_{pitch}	2.2 s
K_{comp}	3 deg/p.u.	T_{comp}	0.1 s
T_{servo}	0.1 s	T_{rl}	0.05 s
$P_{res,max}$	0.1p.u.	$Enable_{res}$	0/1
T_{pick}	10 s	T_{drop}	45 s
$Pitch_{min}$	0 deg	$Pitch_{max}$	27 deg
Up Rate Limit	10p.u./s	Down Rate Limit	−10p.u./s

Table 6
PCO Parameters.

Parameter	Value	Parameter	Value
F_{db}	0.0001 p.u.	R	0.05 p.u.
T_{lag}	1 s	$P_{res,max}$	0.1 p.u.
$Enable_{res}$	0/1	T_{rl}	0.02
Up Rate Limit	0.1 p.u./s	Down Rate Limit	−1 p.u./s

Table 7
Parameters of the "Inertial Emulator" of PV system.

Parameter	Value	Unit	Parameter	Value	Unit
F_{db}	0.0001	p.u.	T_{lag}	0.1	s
K_{ie}	130	–	T_{wo}	0.1	s
T_{rl}	0.0025	s	$Enable_{ie}$	0/1	–
$P_{ie,min}$	0	p.u.	$P_{ie,max}$	0.1	p.u.
Up Rate Limit	1	p.u./s	Down Rate Limit	−1	p.u./s

Table 8
Parameters of the "Inertial Emulator" of BESS.

Parameter	Value	Parameter	Value
F_{db}	0.0001 p.u.	T_{lag}	0.1 s
K_{ie}	130	T_{wo}	0.1 s
T_{rl}	0.005 s	$Enable_{ie}$	0/1
$P_{ie,min}$	0 p.u.	$P_{ie,max}$	0.1 p.u.
Up Rate Limit	1p.u./s	Down Rate Limit	−1p.u./s

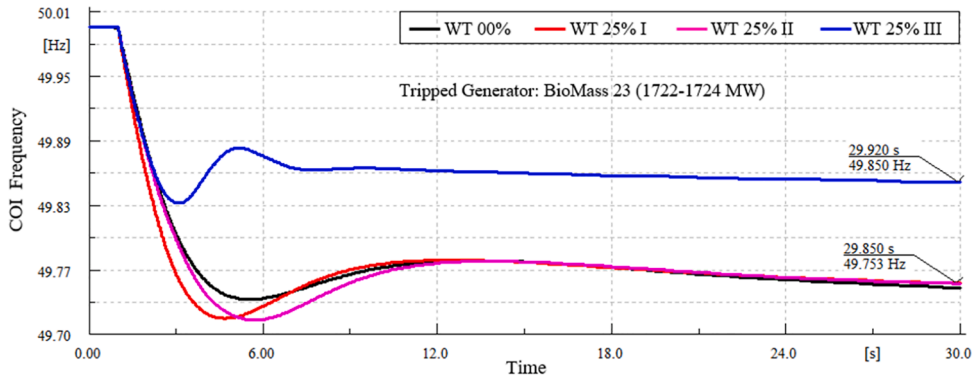

(a)

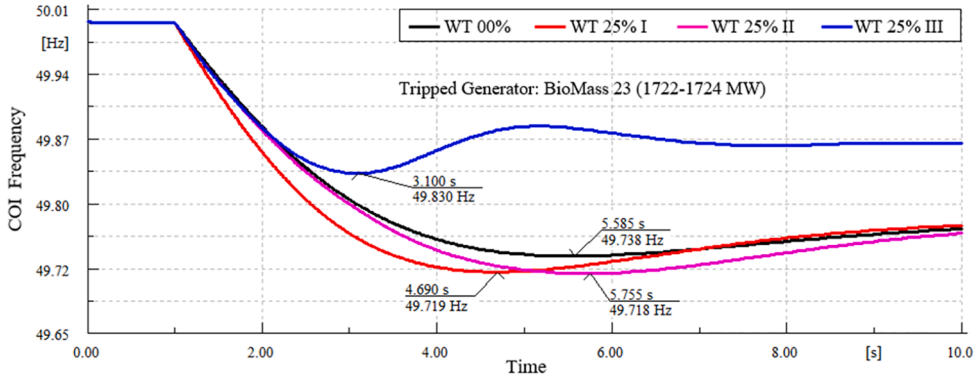

(b)

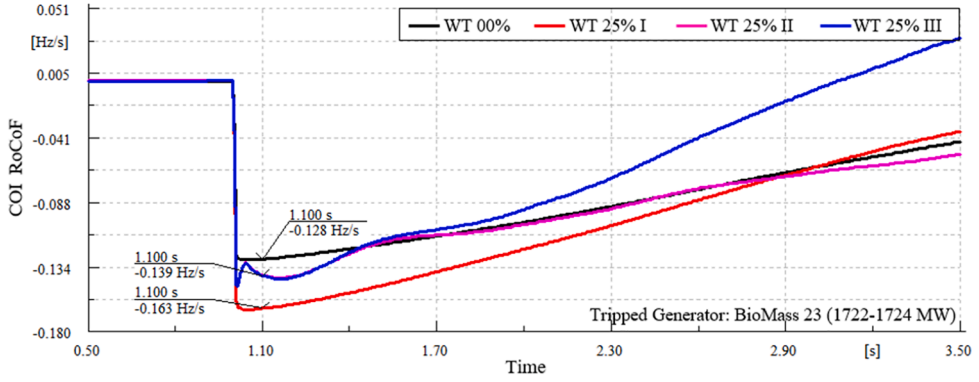

(c)

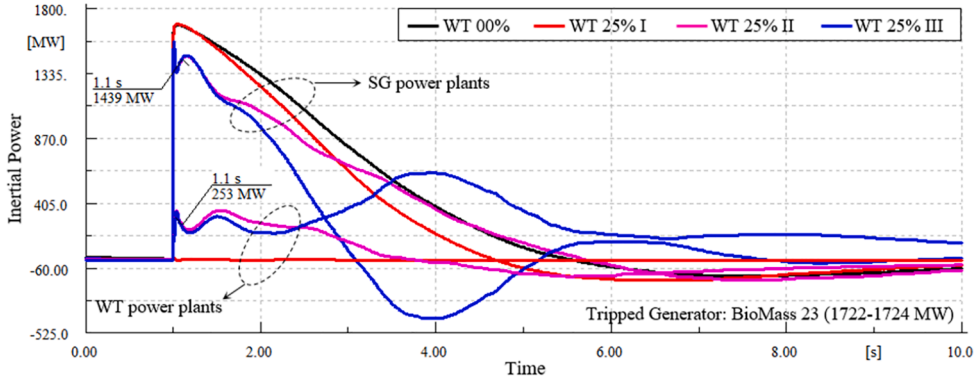

(d)

Fig. 5. (a) Frequency response (b) Frequency nadir, (c) RoCoF deviations, (d) Inertial power changes, and (e) Turbine power deviations; with loss of 1700 MW generation in middle of network (Zone 23).

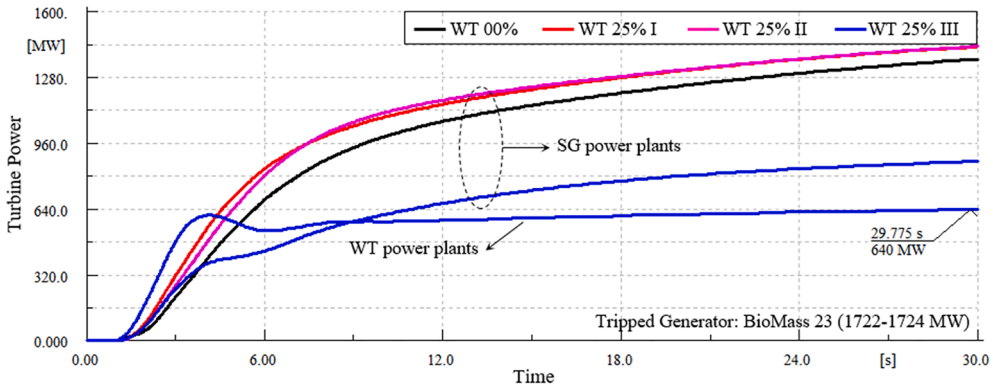

(e)

Fig. 5. (*continued*).

models all the switching procedures results in an overly long simulation time. Therefore, an averaged but accurate model of the PV system is deployed, where the voltage source inverter is treated as a current source in the proposed PV system model. In this way, the simulation time is shortened while at the same time retaining enough precision. Moreover, the PV module physics is modelled accurately. The primary frequency response capability has been integrated into the PV model.

The grid connected two-stage BESS system is deployed and modeled as shown in Fig. 3 (c) [43-46]. The main reason that this model is called two-stage is that two power electronic converters are used in cascade to convert generated power of BESS to AC power. The DC-DC boost converter increases the battery voltage and at the same time a current regulator, controls the active power of BESS by controlling the output current amplitude. In the next stage, a voltage source inverter converts DC link voltage to three phase ac voltage. Finally, the inverter voltage output level increases to the system one using a transformer. However, in order to remove the high frequency harmonics generated by inverter switching, the low pass filter LCL is deployed between inverter and transformer. According to the above-mentioned interpretations, a grid connected BESS is simulated in DIgSILENT PowerFactory so that it can be appropriate for dynamic frequency response of large-scale systems and at the same time the VRB physical modelling is properly modelled. The voltage source inverter is modelled as 'BESS Generator'. Indeed, this is a 'Static Generator' or a simple current source of DIgSILENT PowerFactory software. The power and voltage output of inverter can be measured by 'P Meas' and 'V Meas', respectively. Furthermore, the PLL measures the output frequency of inverter.

The control structure of the WindINERTIA control proposed for GE VSWT model is adopted for 'Inertia Emulator' (See Fig. 4 (a)). Note that in steady state, this controller is not activated. Therefore, it is suitable to add this control signal to the injection power point, as depicted in Fig. 3 (c), as in this architecture, the VSWT will boost its power output immediately. Furthermore, deloading is achieved by pitching blade angle to intentionally spill power, so that the reserve power is deployed for frequency regulation. In a deloaded mode, the pitch angle of a VSWT is made to respond to the frequency changes, akin to the governing function in the conventional units. A proportional control structure (Primary Frequency Support) depicted in Fig. 4 (b) is utilized to generate the supplemental reference angle based on available reserve power. This consists of three main controllers of pitch, pitch compensation and servo motor. The reference angle is determined using the first two controllers in non-reserve power scenario. The servo motor spins the blades with the amount of reference angle. Although the 'Primary Frequency Support' is part of 'WECS Primary Controller', this is located in 'Pitch Controller' due to similarity of PCO in WT and conventional power plant. In 'Primary Frequency Support', the reserve angle of 'Theta_res' is determined based on the available reserve power 'P_res_ava'. 'Theta_res' is the model of MPPT surface in terms of tip speed ratio and pitch angle. The frequency droop control similar to the governing function in a steam turbine as WECS primary controller (PCO) is simulated and shown in Fig. 4 (c). The input signal is the frequency deviation from its nominal value and R is speed regulation parameter or droop parameter, the speed at which the WECS primary controller can act. The governor delay time is Tlag and Presmax is the maximum WT reserve power margin. The rate of change of reserve power is restricted by 'Rate Limiter' block. The relevant parameters are listed in Table 5 and Table 6.

The same inertia emulator and PCO control architecture (Parameters same with WECS's) are deployed for PV and BESS with the parameters shown in Table 7 and 8, respectively.

3. Illustrative Application: WECS

In this section, the frequency response of 36-zone GB network in three sub-scenarios of WT 25 % I (without inertial emulator and pitch controller), WT 25 % II (with inertial emulator and without pitch controller) and WT 25 % III (with inertial emulator and pitch controller) is initially evaluated to show practical applicability of the suggested WECS integrated within 36-zone GB network. Then, the effect of inertial power on dynamic performance of WECS is provided. Furthermore, the influence of wind speed WECS's dynamic variables is presented which conveys many interesting characteristics of the derived WECS in large-scale 36-zone GB network.

3.1. Impact of WECS's primary frequency control

The biomass unit located in zone 23 with the capacity of 1,700 MW is abruptly disconnected. The results are illustrated in Figs. 1 to 3 for WT 00 % and WT 25 % scenarios. The expression (1722–1724 MW) in these figures indicates the loss of generators for these respective two scenarios i.e. 1722 MW and 1724 MW. In order to accurately investigate the WECSs' dynamic performance, the WT 25 % scenario is also divided into three sub-scenarios. In the first sub-scenario WT 25 % I, the inertia

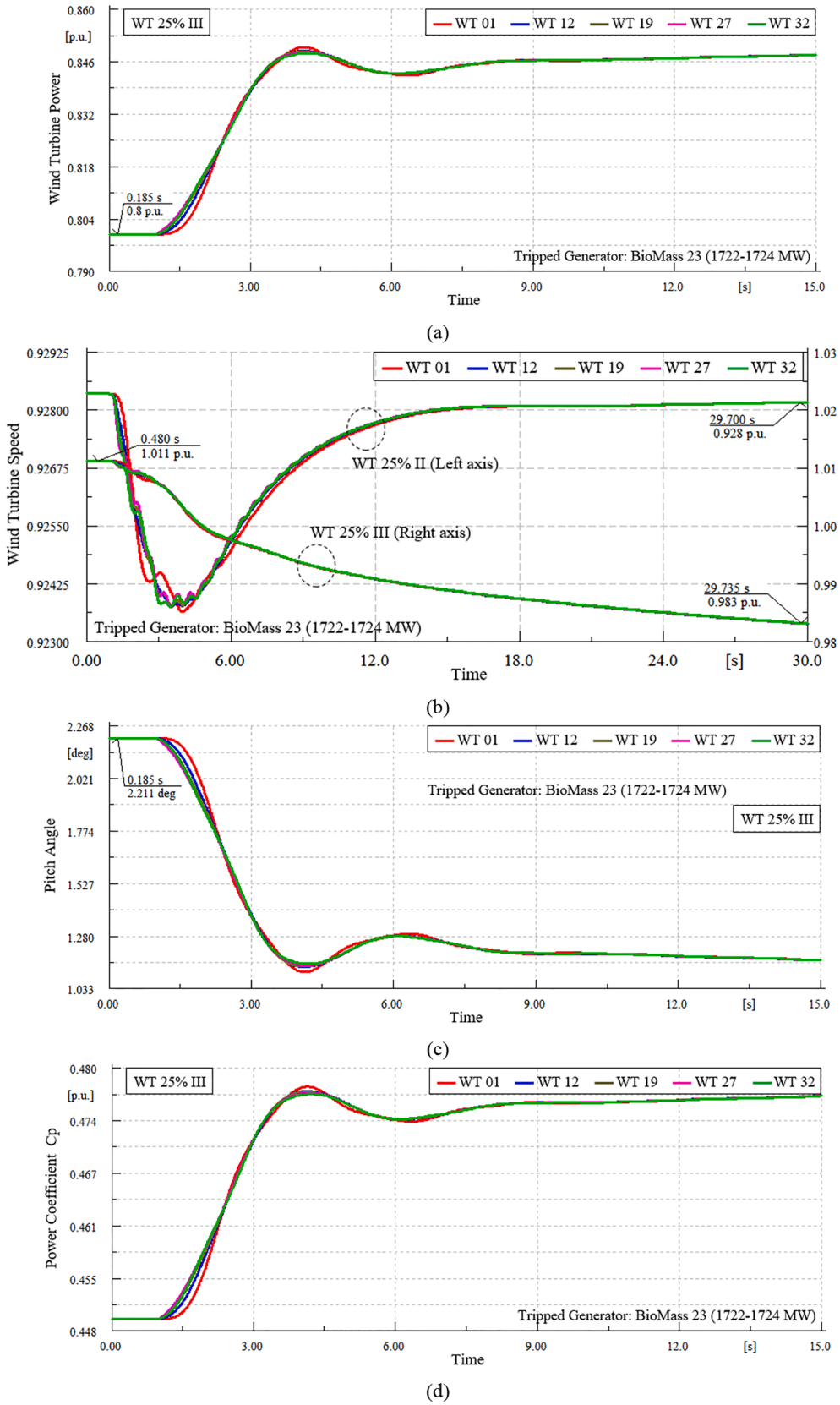

Fig. 6. (a) Wind turbine power changes (b) Wind turbine speed changes, (c) Pitch angle changes, and (d) Power coefficient changes; with loss of 1700 MW generation in middle of network (Zone 23).

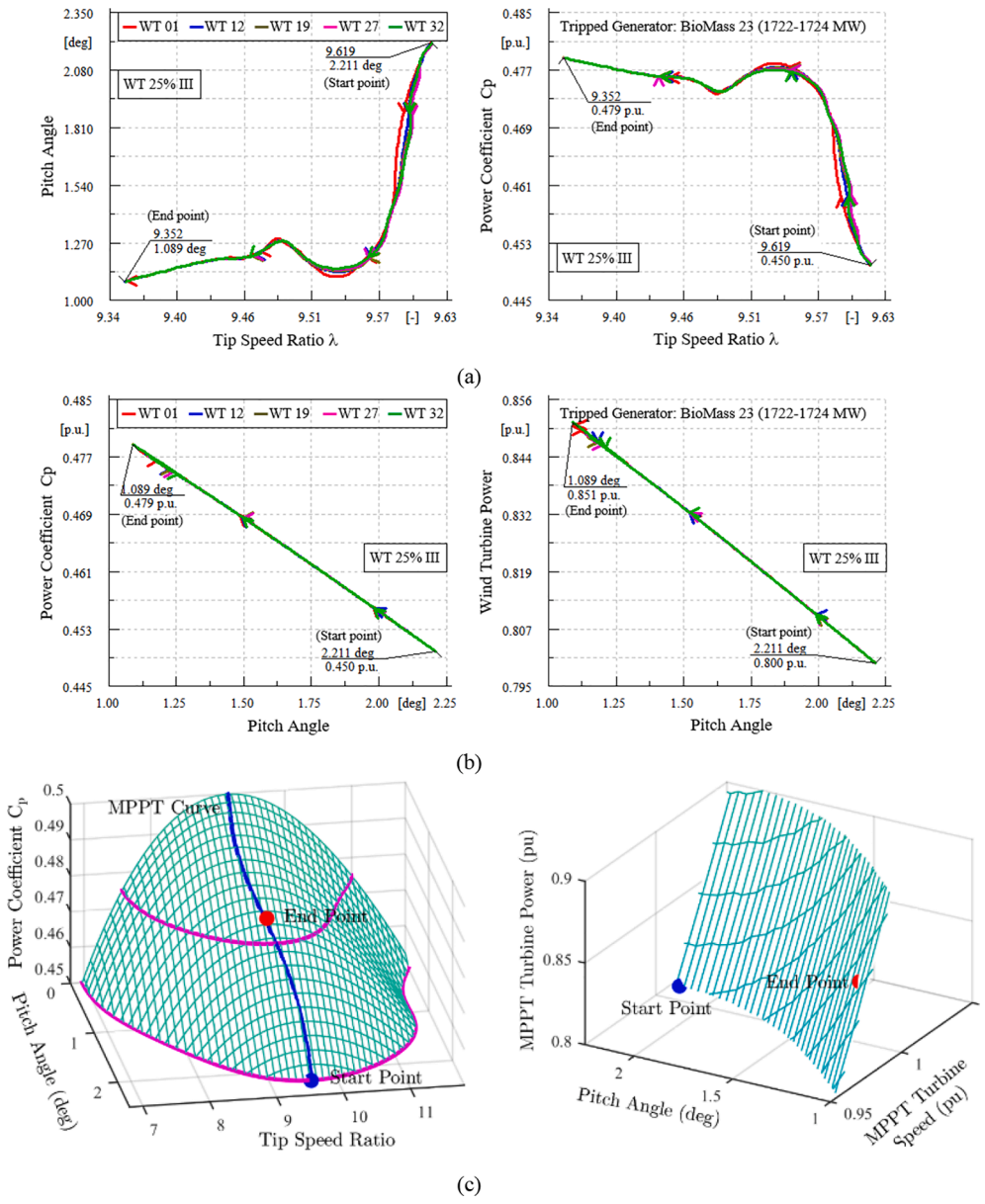

Fig. 7. (a) Pitch angle and power coefficient versus tip speed ratio trajectories (b) Power coefficient and wind turbine power versus pitch angle trajectories, and (d) Location of pre- and post-event operating points of WECSs on MPPT characteristics: Power coefficient versus pitch angle and tip speed ratio (Left) and MPPT turbine power versus pitch angle and MPPT turbine speed (Right); with loss of 1700 MW generation in middle of network (Zone 23).

emulator and PCO are deactivated for all WECSs. It means that the power output of WECS is independent of network frequency deviation, and it is fixed in both pre- and post-contingency states. In the second sub-scenario WT 25 % II, all inertial emulators are activated for all WECSs. Therefore, they are able to instantaneously inject power so-called 'Inertial Power' to the network following the event in order to reduce the RoCoF of center of inertia (COI). It is notable that the main idea of the controller is to respond quickly to frequency variation and enhance the frequency nadir as well as RoCoF. In last sub-scenario WT 25 % III, both PCO and inertial emulator are activated to provide ancillary services to frequency event. Whilst both synchronous (PCO) and emulated inertial responses of WECSs act in the time-frame before the full governor droop response provision, there is a delay due to a dead-band in inertial emulator to prevent false triggering. It is to be noticed that PCO is considered to support the WECSs for participating in the frequency response and the WECSs should operate at partial load, ensuring sufficient reserve power at any instant. This is de-loading mode that can be deployed to tune the active power output of WT by rotor speed control. Then, the active power obtained by each WT can drop down or up to complement the system frequency deviations. It is also notable that this power is injected simultaneously with inertial power following the in-feed.

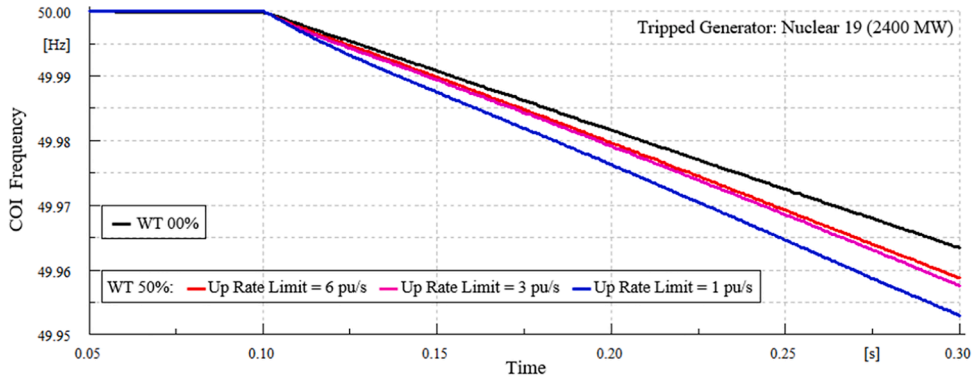

(a)

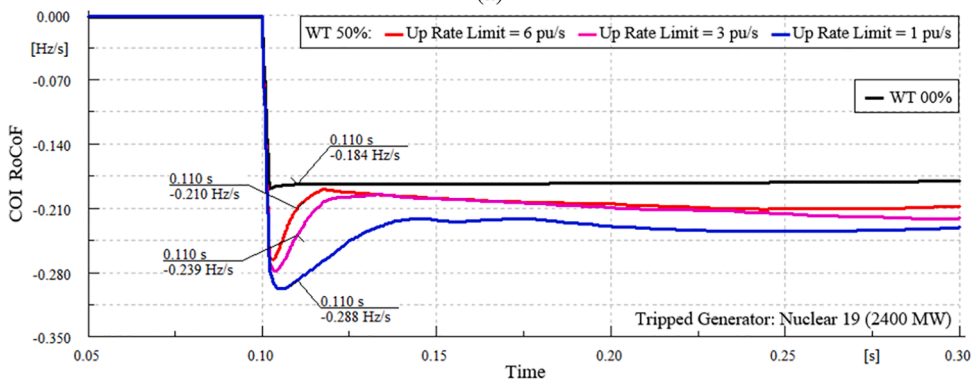

(b)

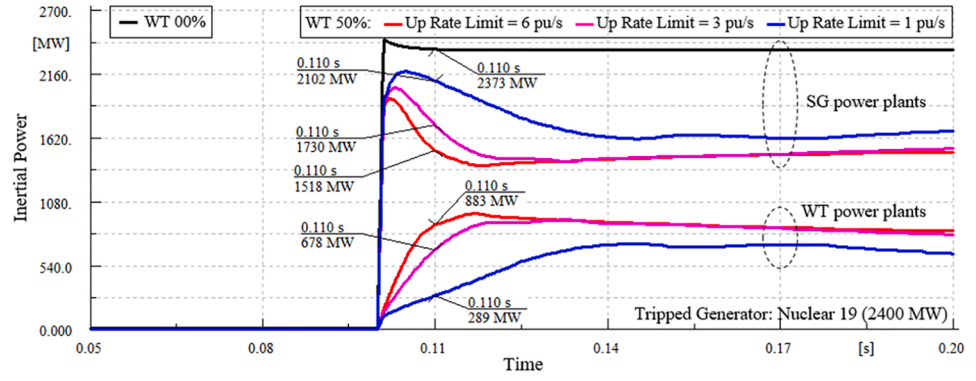

(c)

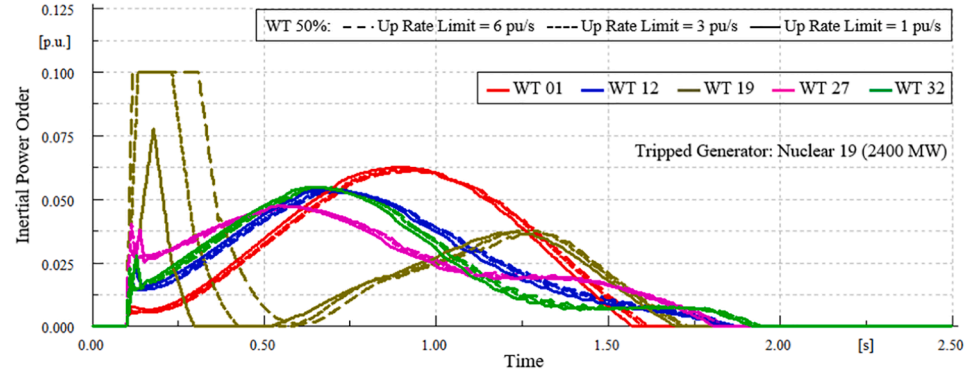

(d)

Fig. 8. (a) Frequency response; (b) RoCoF deviations; (c) Inertial power changes; (d) Inertial power order changes; (e) Up rate limits of inertial power order; and (f) Wind turbine speed changes; all for comparing different up rate limits of inertial emulator.

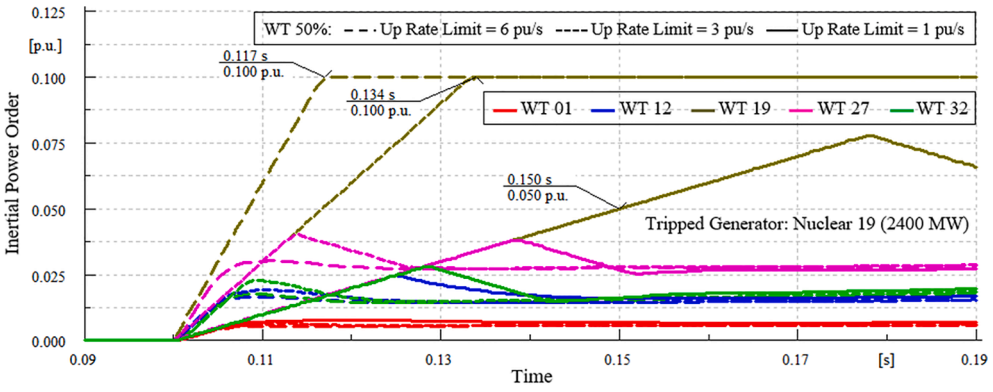

(e)

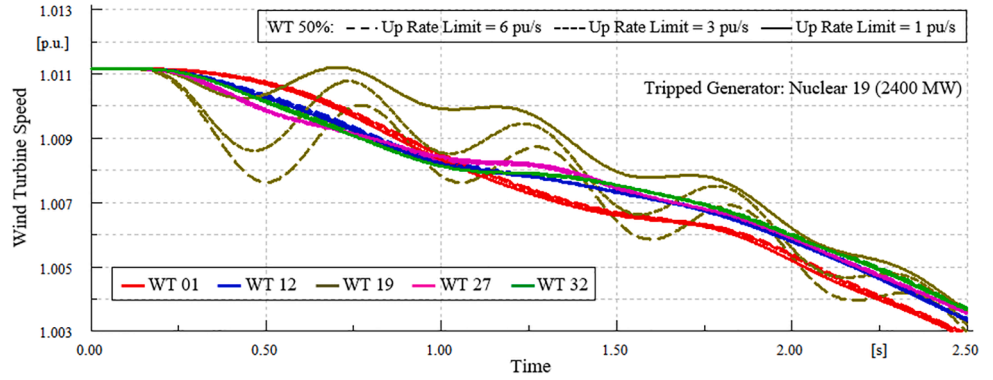

(f)

Fig. 8. (*continued*).

The COI frequency change for the above-mentioned four scenarios is shown in Fig. 5 (a) and (b). The COI RoCoF variation for the first few seconds after the event is portrayed in Fig. 5 (b). Fig. 5 (d) shows the initial power of all conventional (SG power plants) and all WT units (WT power plants) in 36-zone GB network. The turbine power deviations with respect to pre-contingency state are plotted in Fig. 5 (e) for both conventional and WECS power plants. Based on Fig. 5 (a) and (b), it can be seen that system frequency of WT 00 % scenario is more than WT 25 % I for the first six seconds following the disturbance, while it is less than that after this interval. As can be seen from Fig. 5 (e), the main reason for this phenomenon is that the initial power in WT 25 % I is less than WT 00 % due to replacement of gas turbines with WECSs without inertial emulator. Consequently, this can lead to the situation that COI RoCoF in WT 25 % I scenario is more than other, as shown in Fig. 5 (d). For the sake of comparison of system frequency for the interval 4 to 30 s, the system frequency of WT 25 % I should be apparently less than that of WT 00 % since some of conventional units are replaced with WECSs which are not equipped with reserve power. However, as it can be seen from Fig. 5 (a) and (b), it is not true. The main reason for this matter is that WTs are replaced with CCGTs. These units work based on their base load operation mode before the disturbance and their power outputs will be dropped down following the frequency excursion. As a result, the replacement of these power plants with WECSs (Even WECSs without primary frequency support ability) can enhance primary frequency control support. Moreover, the SGs' turbine power in WT 25 % I is less than those of WT 00 % scenario, as depicted in Fig. 5 (e). Therefore, the steady state value of frequency in first scenario is more than the second one.

In scenario WT 25 % II, the inertial emulator of all WECSs are activated. Therefore, as can be seen from Fig. 5 (d), all WECSs inject inertial power to grid following the event. This can reduce COI RoCoF with respect to WT 25 % I. However, the frequency nadir and steady-state value of frequency are not changed compared to WT 25 % I since reserve power is neglected for WECSs. Finally, all PCO blocks are activated in WT 25 % III scenario and reserve power is incorporated. The R parameter in PCO block is 0.05 for all WECSs. As a result, 640 MW out of 1,500 MW primary frequency responses is generated by WECSs in this scenario. This reduces frequency nadir and its steady state value by 40 % and 40 % compared to WT 25 % II scenario.

In order to more efficiently investigate the frequency response of WECSs, several quantities related to frequency response of 5 WECSs depicted in Fig. 2 (b) are shown in Figs. 6 and 7. The turbine power change of WECSs is plotted in Fig. 6 (a) for WT 25 % III scenario. It is to be noticed that before the event, the WECSs intentionally spill power and work on power equal 0.8p.u. (Partial mode), so that the reserve energy can be used for frequency regulation, akin to the governing function. It is the reason that power outputs of WECSs are proportionally increased. Additionally, WT spinning speed variations for two scenarios of WT 25 % II and WT 25 % III are shown in Fig. 6 (b). As can be seen, in former scenario, since WECSs just inject inertial power to the grid, the WT speed is reduced for the first second after event occurrence and then turns back to the previous value preceding a transient state. In contrast, in WT 25 % III scenario where all WTs operate at partial load with a de-loading margin (reserve power) of 10 %, the equilibrium points of WTs' powers are changed in pre- or post-contingency states. Thus, WTs' speed

Table 9
Percentage of wind speed deviations in wind speed scenarios.

Scenarios	Area 01	Area 02	Area 03	Area 04	Area 05
Wind Speed I	0 %	0 %	0 %	0 %	0 %
Wind Speed II	−5 %	2 %	−10 %	3 %	−5 %
Wind Speed III	−5 %	−4 %	−5 %	−2 %	−5 %

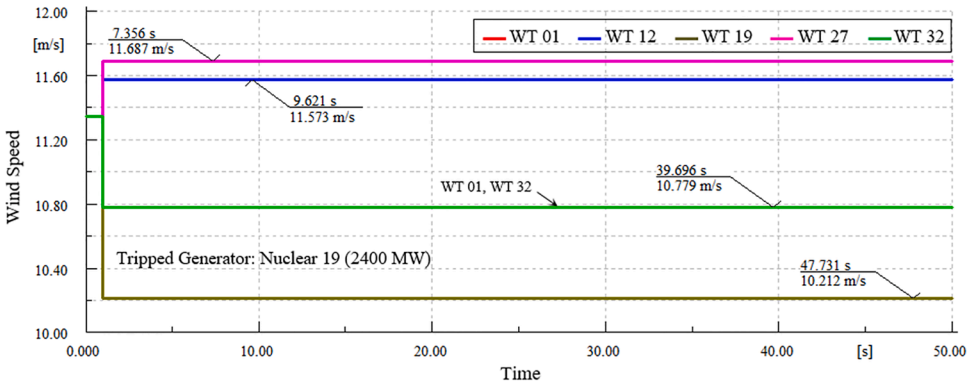

(a)

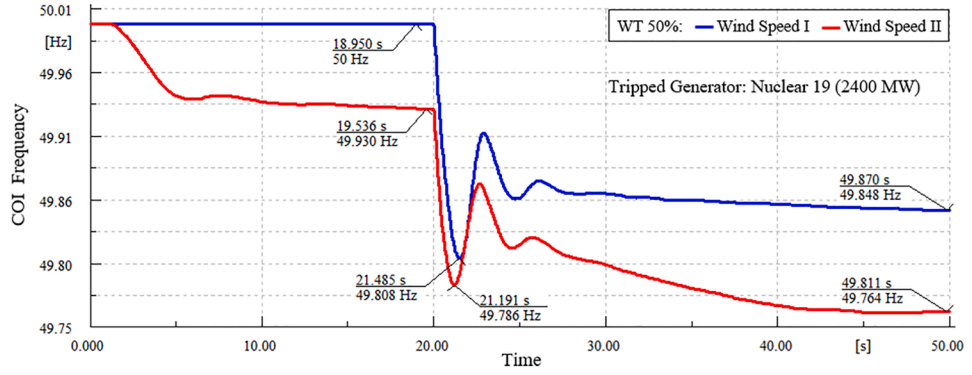

(b)

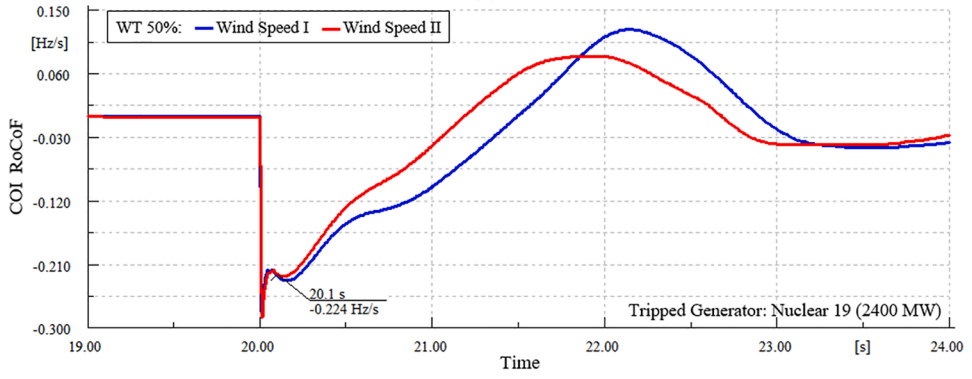

(c)

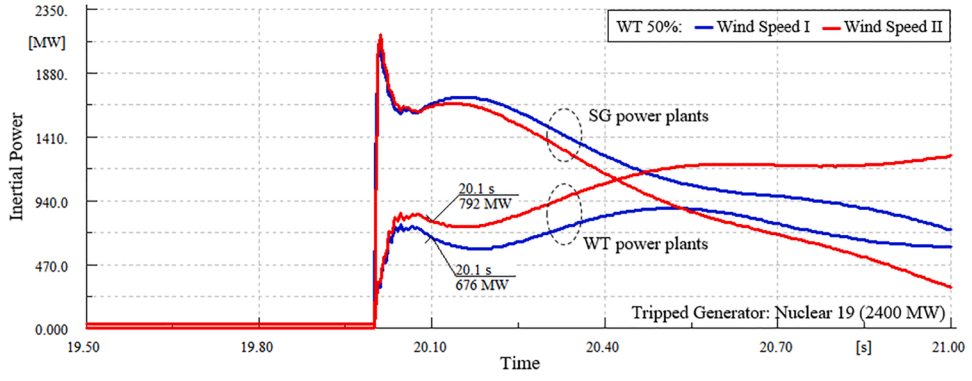

(d)

Fig. 9. (a) Wind speed of wind turbines in Wind Speed II scenario (b) Frequency responses, (c) RoCoF deviations, (d) Inertial power changes, (e) Turbine power deviations, (f) Wind turbine reserve power changes of area 01, area 02, area 04 and area 05, and (g) Wind turbine reserve power changes of area 03 and all areas; in "Wind Speed I" and "Wind Speed II" scenarios.

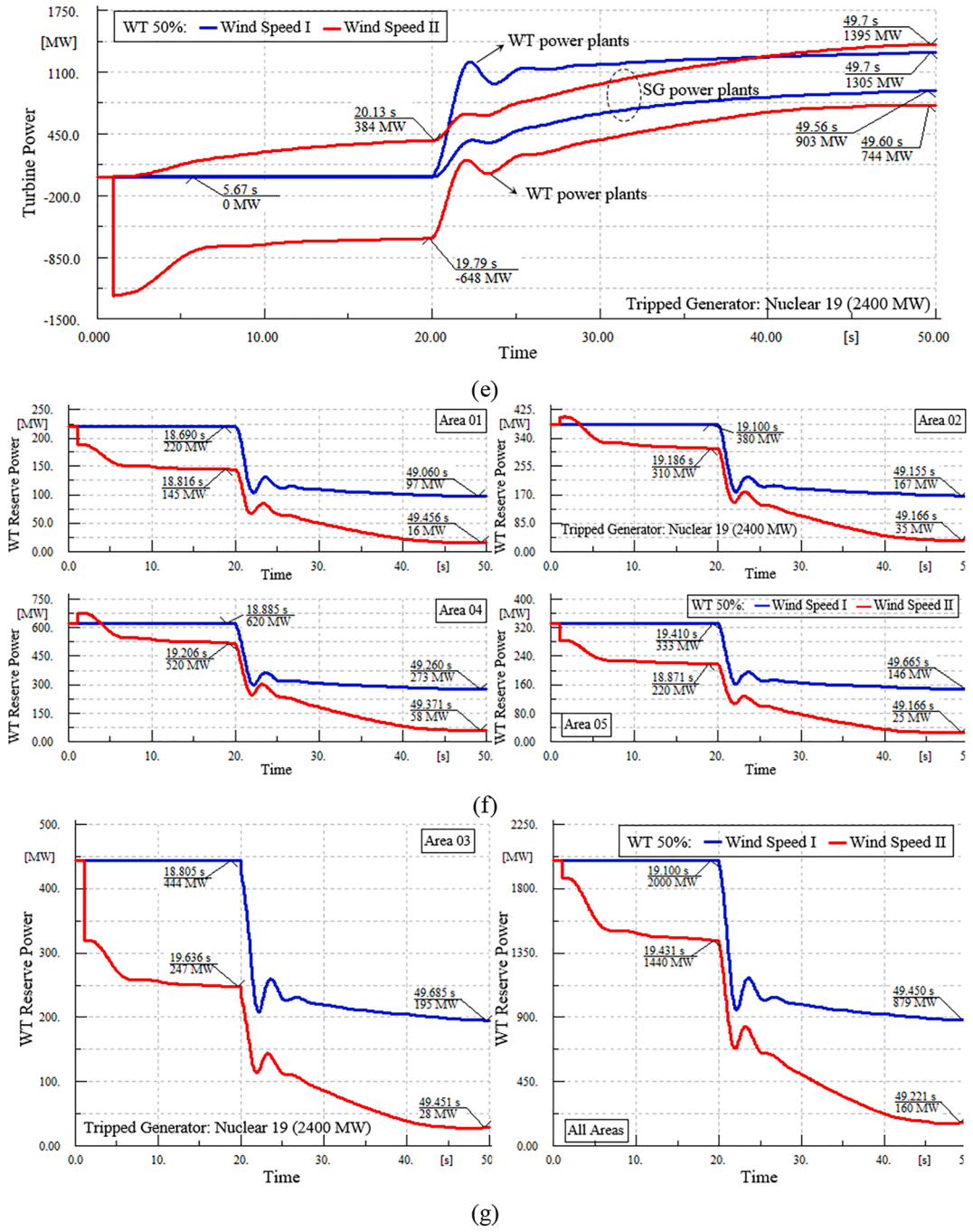

Fig. 9. (*continued*).

for post-contingency state after transient procedure is different from pre-contingency state. Moreover, like the second event, the WT speed after the vent is less than before that in this loss of generator. What should also be underscored is that WT's speed oscillation for the first moments following the event is less than those of first and second events. This is because despite the first and second incidents, none of 5 WECSs specified in Fig. 2 (b) are not located near to the event location i.e. zone 23. In other hand, the same rotor oscillation to the first and second events should be observed in WT speed of WECS located in zone 23.

As it has been discussed above, the pitch angle of WTs' blades is tuned in a value bigger than zero to keep the additional available power as reserve. This implementation will add to the pitch compensation process and will guarantee modifications in the mechanical power captured from the wind by reducing the pitch angle to provide additional power to the grid following the loss of generator. It means that the power coefficient (C_P) adjusts for a given blade pitch angle. As a result,

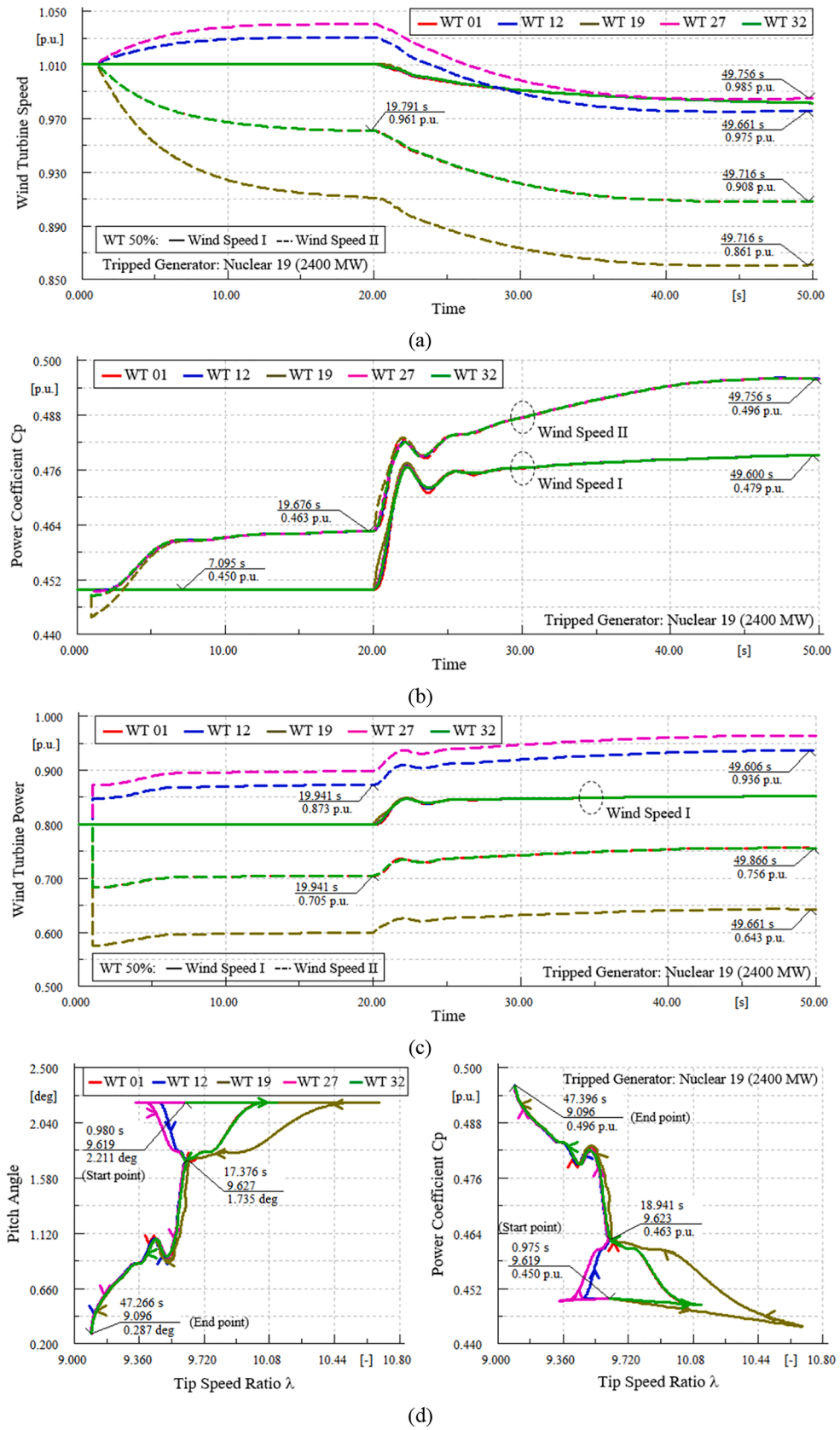

Fig. 10. (a) Wind turbine speed changes (b) Power coefficient changes, (c) Wind turbine power changes, (d) Pitch angle and power coefficient versus tip speed ratio trajectories, and (e) Location of pre- and post-event operating points of WECSs on MPPT characteristics: Power coefficient versus pitch angle and tip speed ratio (Left), MPPT turbine power versus pitch angle and MPPT turbine speed (Right); in "Wind Speed I" and "Wind Speed II" scenarios.

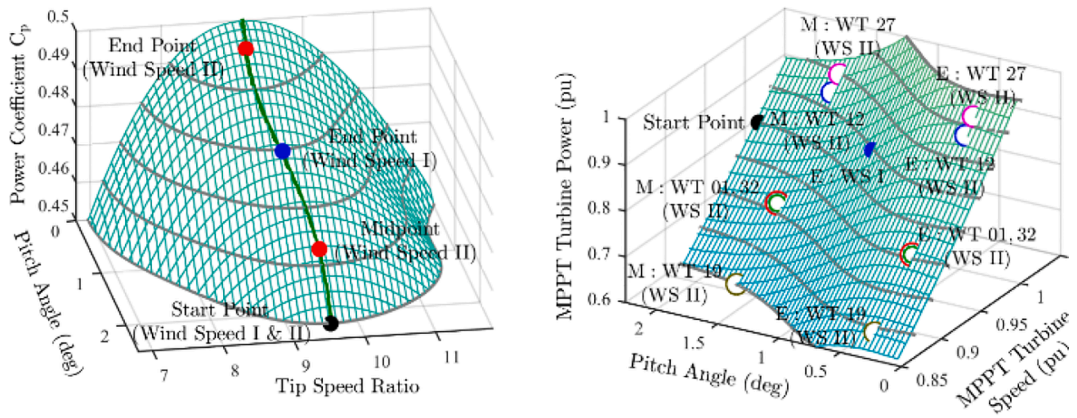

(e)

Fig. 10. (*continued*).

the WT's power output is changed based on C_P proportionally. The pitch angle and C_P change for five WECSs are respectively shown in Fig. 6 (c) and (d). It is clear-cut that pitch angles of WTs reduce approximately from 2.1° to 1.1° so that C_P is consequently increased from 0.45 to 0.48.

In order to monitor the change of equilibrium point for WTs before and after the loss of generation, four trajectories related to five above-mentioned WECSs are shown in Fig. 7 (a) to (c). Moreover, the WECSs' equilibrium point in pre- and post-contingency state is shown on MPPT curve in Fig. 7 (c). These trajectories are related to WT 25 % III scenario. The pitch angle versus tip speed ratio is shown in left hand side of Fig. 7 (a). The power coefficient versus tip speed ratio trajectory is shown in right hand side of Fig. 7 (a). As tip speed ratio (λ) is correlated with the ratio of rotor speed over wind speed and wind speed is fixed in this study, the oscillation observed in trajectories illustrated in Fig. 7 (a) causes by rotor speed oscillation. In contrast, power coefficient and turbine power versus angle trajectories are portrayed in Fig. 7 (b). Despite the trajectories of Fig. 7 (a), a linear relationship is observed in trajectories of Fig. 7 (b). It is to be noted that power coefficient and turbine power are increased in proportion to pitch angle reduction. The start points of Fig. 7 (a) and (b) correspond to blue points in Fig. 7 (c). In this point, the reserve power of WECSs is 10 % of its generated power. In other hand, the end point shown in Fig. 7 (a) and (b) is corresponded to red points in Fig. 7 (c). In this point, 6 % out of 10 % of reserve power is injected to the network. It is also notable that WT's speed reduction observed following the disturbance can be justified with the smaller value of tip speed ratio at the end point of left-hand side curve of Fig. 7 (c).

3.2. Impact of wind inertia power

In all previous case studies, the effect of different values of wind penetration level as well as reserve power of WECSs on GB system frequency response is investigated. In all these circumstances, it is observed that COI RoCoF is raised by increasing these criteria. In other words, albeit the increment rate of primary frequency response of WECSs is more than conventional units, the rate of inertial power increment of WECSs is limited to 1p.u./s which is less than conventional units. In this regard, the impact of inertial power increment rate of WECSs on 36-zone GB system COI RoCoF is evaluated. The considered event is that the nuclear unit located in zone 19 with the capacity of 2,400 MW is abruptly disconnected. The penetration level is fixed to 50 %. The GB system frequency response for the initial moments of event occurrence for different values of 'Up Rate Limit' in Inertial Emulator blocks of WECSs are illustrated in Fig. 8. For the sake of better comparison, the results of WT 00 % scenario are also appended into the figures. The change of COI frequency and COI RoCoF are portrayed in Fig. 8 (a) and (b). It is clear-cut that the RoCoF is reduced with increasing inertial power rate of WECSs. To be accurate, the RoCoF values drop by 17 % and 27 % with the Up Rate Limit growth from 1pu/s to 3 pu/s and 1pu/s to 6 pu/s, respectively, as shown in Fig. 8 (c).

In order to more efficiently investigate the frequency response of WECSs under different values of initial power increment rate, several quantities related to frequency response of 5 WECSs are shown in Fig. 8 (d) to (f). The inertial power order change extracted from inertial emulator block is plotted in Fig. 8 (d). In this figure, the lower and upper limits of this signal are 0 and 0.1 pu, respectively. As can be seen, the closest WT to the event i.e. WT 19 is reached to the upper limitation. The initial times following the disturbance are zoomed in Fig. 8 (e). This figure evidently shows that the considered Up rate limit is quite matched with WT located in zone 19. In addition, it is quite clear that the algebraic summation of all WECSs of GB network is 20 GW or 25 GVA with power factor of 0.8. Therefore, the inertial power of WECSs needs to be increased by 25 GW per second or 250 MW per 0.01 s for Up rate limit equal to 1 pu/s. The corresponding values for Up rate limits of 3 and 6 should be made 3 times and 6 times. The numerical values specified in Fig. 8 (c) for WECS with Up rate limit of 1 and 3 have 15 % and 10 % difference with pre-determined values. This is due to terminal voltage change of WECSs and their active power variation in consequence. However, this difference is 40 % for Up rate limit of 6. In other word, the analytical value of inertial power for WECSs should be 1500 MW per 0.01 s, however, this value is 880 MW based on Fig. 8 (c). In order to clarify this matter, two vital items need to be pointed out:

i) The value of 1500 MW is the maximum inertial power for WECSs not the necessary amount. It means it is possible that the generation lost value is small so that system RoCoF can't change the inertial power increment rate of all WECSs to this maximum limit.
ii) It is possible that the WT distance to the incident is huge and the local RoCoF measured by this unit can't change the inertial power increment rate of all WECSs to this maximum limit. This pint is illustrated in Fig. 8 (c) so that in case of Up rate limit of 6 pu/s, the only unit's inertial power which is reached to the maximum value is WT located

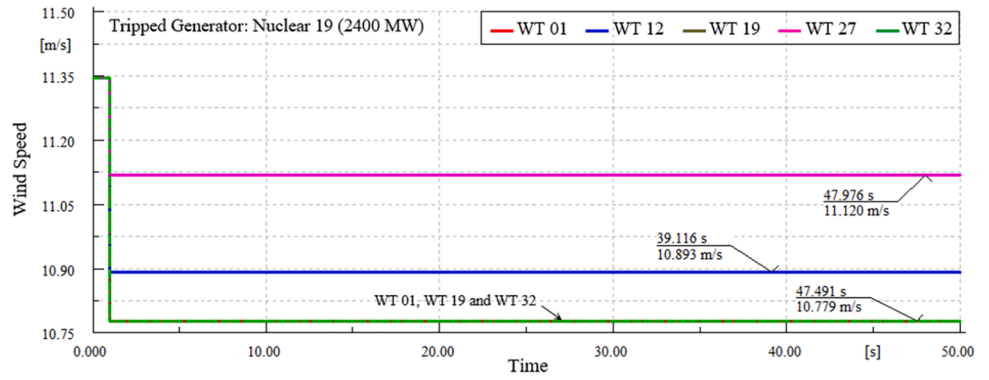

(a)

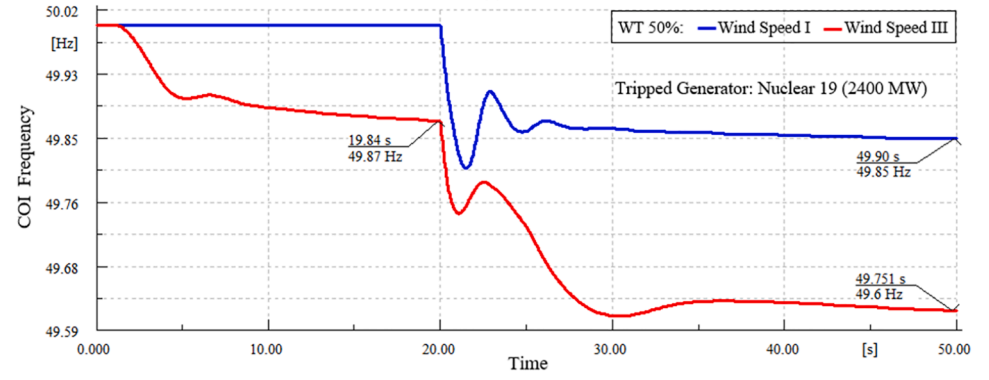

(b)

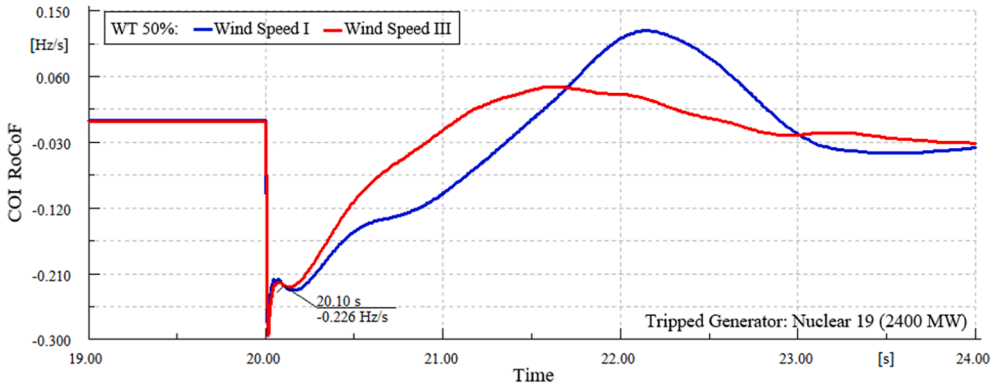

(c)

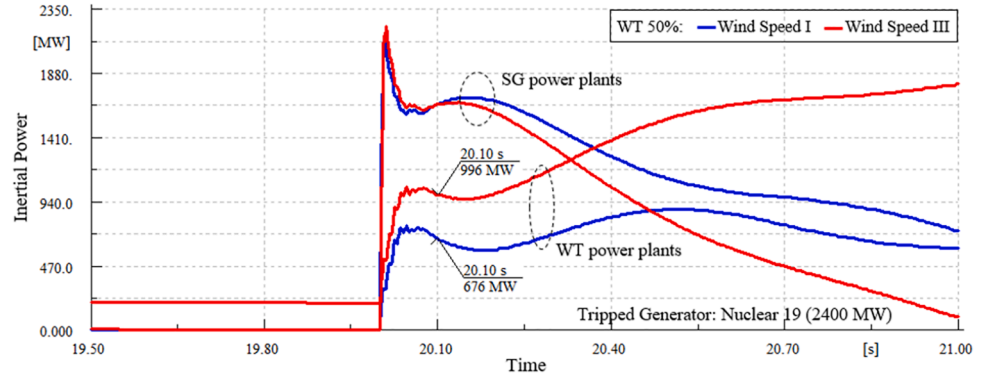

(d)

Fig. 11. (a) Wind speed of wind turbines in Wind Speed III scenario (b) Frequency responses, (c) RoCoF deviations, (d) Inertial power changes, (e) Turbine power deviations, (f) Wind turbine reserve power changes of area 01, area 02, area 04 and area 05, and (g) Wind turbine reserve power changes of area 03 and all areas; in "Wind Speed I" and "Wind Speed III" scenarios.

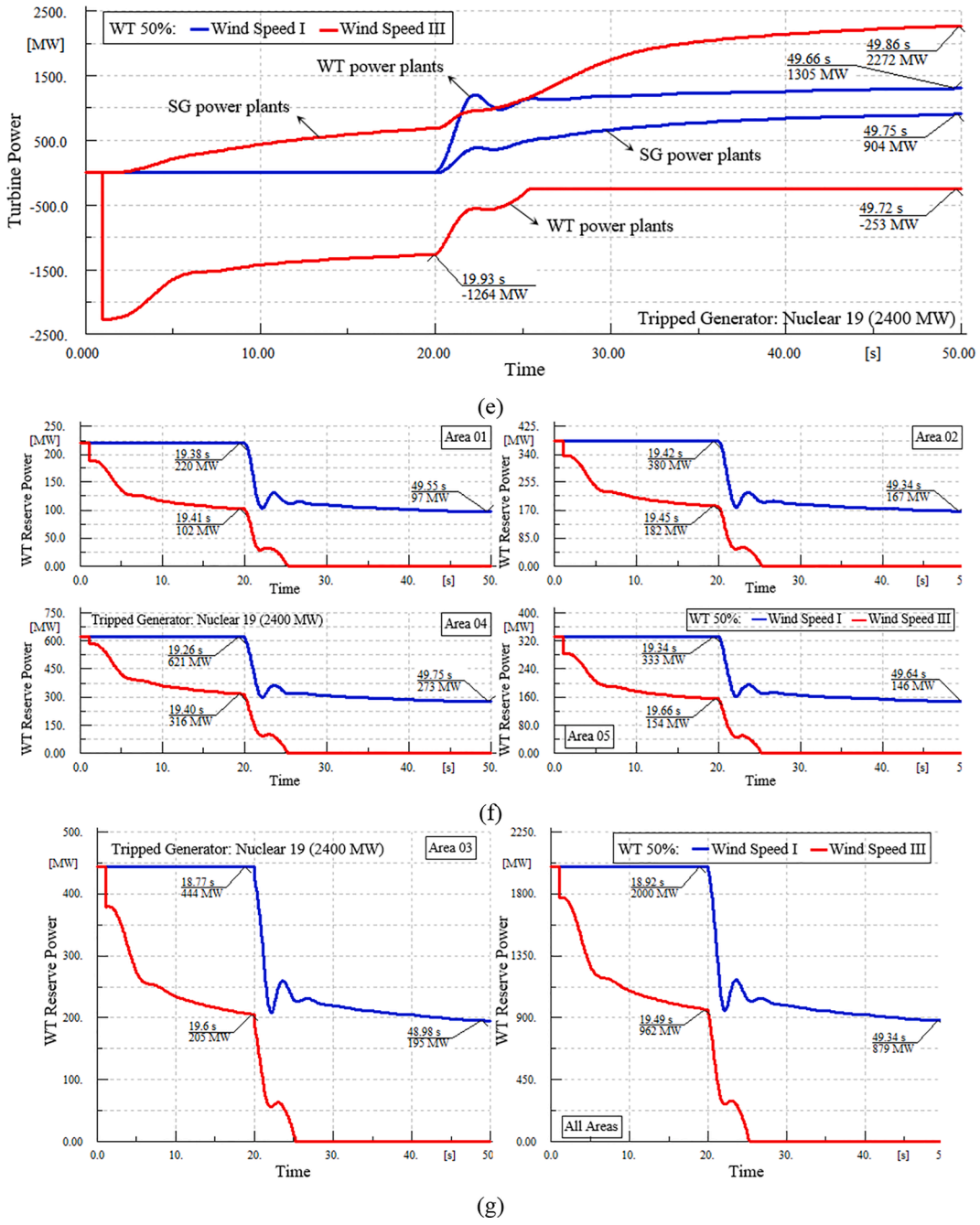

Fig. 11. (*continued*).

beside the disturbance in zone 19. Therefore, the inertial power of this unit needs to be less than 1500 MW in this case.

The WT speed for the first moments of event is depicted in Fig. 8 (f) for discrepant values of Up rate limit. What should be underscored is that whilst the COI RoCoF is reduced with increasing the inertial power rate increment, the WT rotor oscillation especially for the WECSs located nearer to the in-feed is increased.

3.3. Impact of wind speed on frequency response

In order to solve load flow problem, the power generated by WECSs are tuned in to a known value in DIgSILENT PowerFactory. After which, wind speed is determined based on this power as well as assigned value to reserve power. However, in practice, wind speed determines the generated power and its reserve for each WECS. To further demonstrate the effectiveness and applicability of the proposed control in practical cases, the GB system frequency response is investigated considering

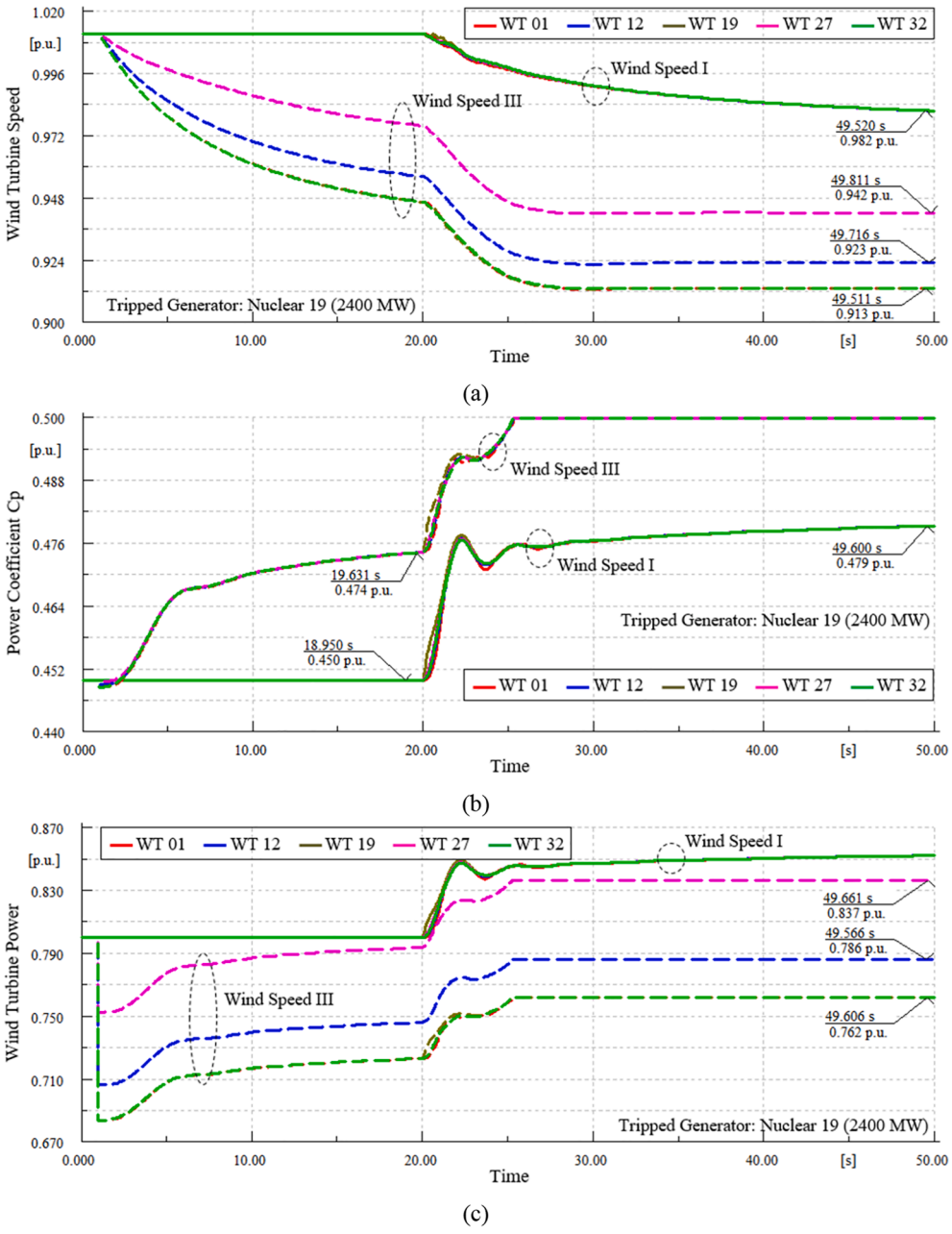

Fig. 12. (a) Wind turbine speed changes (b) Power coefficient changes, (c) Wind turbine power changes, (d) Pitch angle and power coefficient versus tip speed ratio trajectories, and (e) Location of pre- and post-event operating points of WECSs on MPPT characteristics: Power coefficient versus pitch angle and tip speed ratio (Left), MPPT turbine power versus pitch angle and MPPT turbine speed (Right); in "Wind Speed I" and "Wind Speed III" scenarios.

discrepant scenarios for wind speed. The penetration level of WECSs in this scenario is 50 % and reserve power margin of 10 % is assigned to all of them. The wind speed deviations percentage of five different areas depicted in Fig. 2 (b) are tabulated in Table 9 for three scenarios. The wind speed of all regions in all time horizon is fixed in Wind Speed I scenario. In Wind Speed II scenario, the wind speed is dropped down in some areas and decreased in others. It means that wind speed is increased in zones 2 and 4 and reduced in other three regions. The maximum drop is intentionally considered as −10 % in zone 3. Finally, the worst case in terms of available reserve power is simulated in Wind speed III with wind speed reduction of all areas.

- First Case: Increasing/Decreasing Wind Speed of All WECSs

In this subsection, the 36-zone GB system frequency response for the scenario of Wind Speed II following the loss of nuclear power (2,400 MW) located in zone 19 is investigated. The relevant results beside Wind Speed I scenario are illustrated in Figs. 9 and 10. The simulation time interval is 50 s. Moreover, wind speed values are changed at $t = 1$ s for all five regions depicted in Fig. 2 (b), as shown in Fig. 9 (a). The

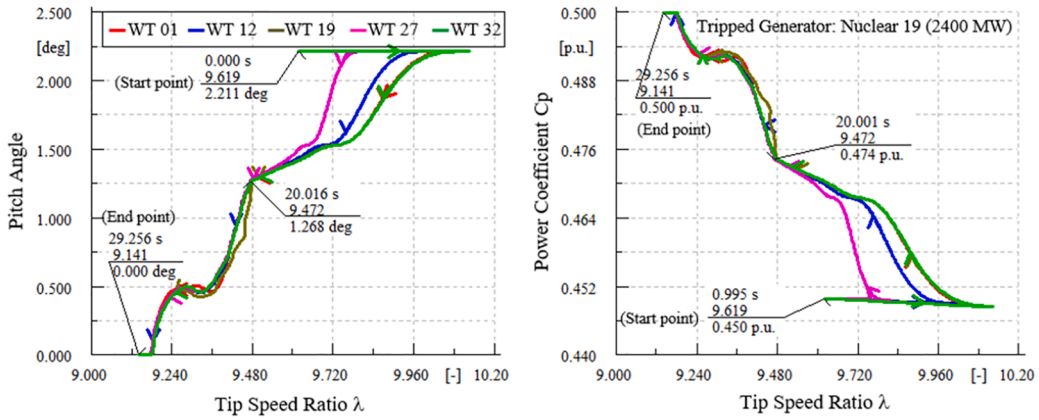

(d)

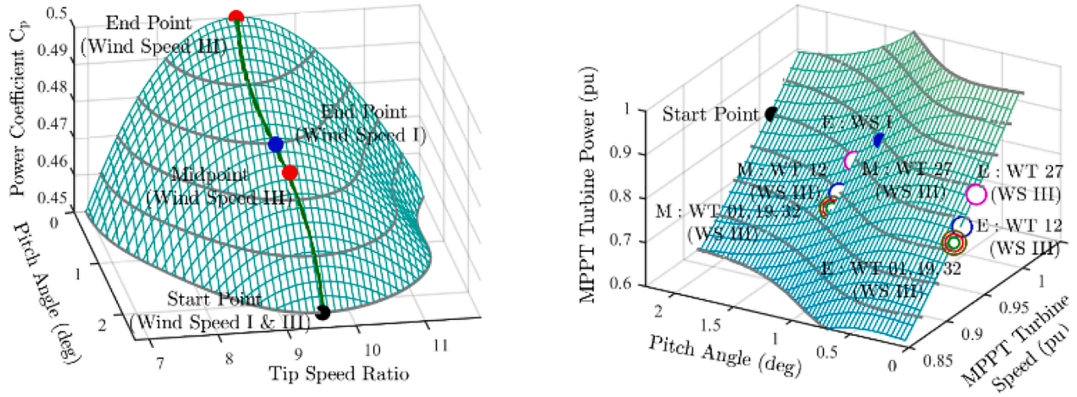

(e)

Fig. 12. (*continued*).

maximum wind speed reduction of −10 % is related to Area 03 where disturbance location is located in zone 19. The loss of generator is simulated at $t = 20$ s.

The COI frequency and COI RoCoF of GB network are shown in Fig. 9 (b) and (c), respectively. Furthermore, the inertial power variations of conventional unit as well as WECS are illustrated in Fig. 9 (d) for the initial times of disturbance occurrence. Fig. 9 (e) illustrates conventional and WT turbine power change. As discussed above, the wind speed variation can change power generated by WECSs and vary reserve power, consequently. In this context, the reserve powers of all 5 regions depicted in Fig. 2 (b) are shown in Fig. 9 (f) and (g) including their algebraic summation. The reserve power variations of all four regions where the disturbance has not happened, are shown in Fig. 9 (f). On the other hand, the corresponding values of Area 03 (Disturbance is occurred in this region) and the power summation of all areas are shown in Fig. 9 (g) for Wind Speed I and Wind Speed II scenarios.

Applying the wind speed change of Wind Speed II depicted in Fig. 9 (a) on WECSs leads to output power reduction of WECSs by 1,200 MW. This in turn can abruptly mitigate reserve power of WECSs, as shown in Fig. 9 (f) and (g). As can be seen from right hand side of Fig. 9 (g), the amount of this reduction for the whole network is 120 MW which is quite matched to 10 % reserve power of WECSs. This wind speed variation is like loss of wind power leading to system frequency mitigation, as depicted in Fig. 9 (b). Due to this fact, output powers of conventional units and WECSs increase following the event as shown in Fig. 9 (e). As a result, some part of WECSs' reserve power is occupied to compensate WECSs' power reduction in consequence of wind speed changes. The reserve power of WECSs reduces by 28 % from 2000 MW to 1440 MW in $t = 20$ s. This is because the frequency nadir and steady-state frequency deviation in Wind Speed II scenario dropped down by 11 % and 60 % compared to Wind Speed I, respectively. However, the COI RoCoF is equal in both scenarios. Note, the residual reserve power of all WECS is 160 MW at the end of simulation time.

In order to accurately investigate the above matter, some quantities related to 5 WECSs, are shown in Fig. 10 (a) to (e). The rotor speed, power coefficient and turbine power variations of WECSs are portrayed in Fig. 10 (a), (b) and (c), respectively. Furthermore, pitch angle and power coefficient versus tip speed ratio trajectories are plotted in Fig. 10 (d) for Wind Speed (WS) II scenario. The equilibrium points of 5 WECSs on MPPT curves are determined for three times of start point, midpoint (M) and end point (E) which are 0 s, 20 s and 50 s, respectively. It is clear that the sudden increment and decrement of wind speed in $t = 1$ led to rotor speed boost and buck, respectively. This can be justified based on tip speed ratio equality of initial and mid equilibrium points of left-hand side of Fig. 10 (e) in Wind Speed II ratio. It is to be notified that five WECSs have dissimilar rotor speed and identical pitch angle in $t = 20$ s. These can be observed in left- and right-hand side of Fig. 10 (d) and (e), respectively. It is noteworthy that 2.5 % out of 10 % of reserve power of

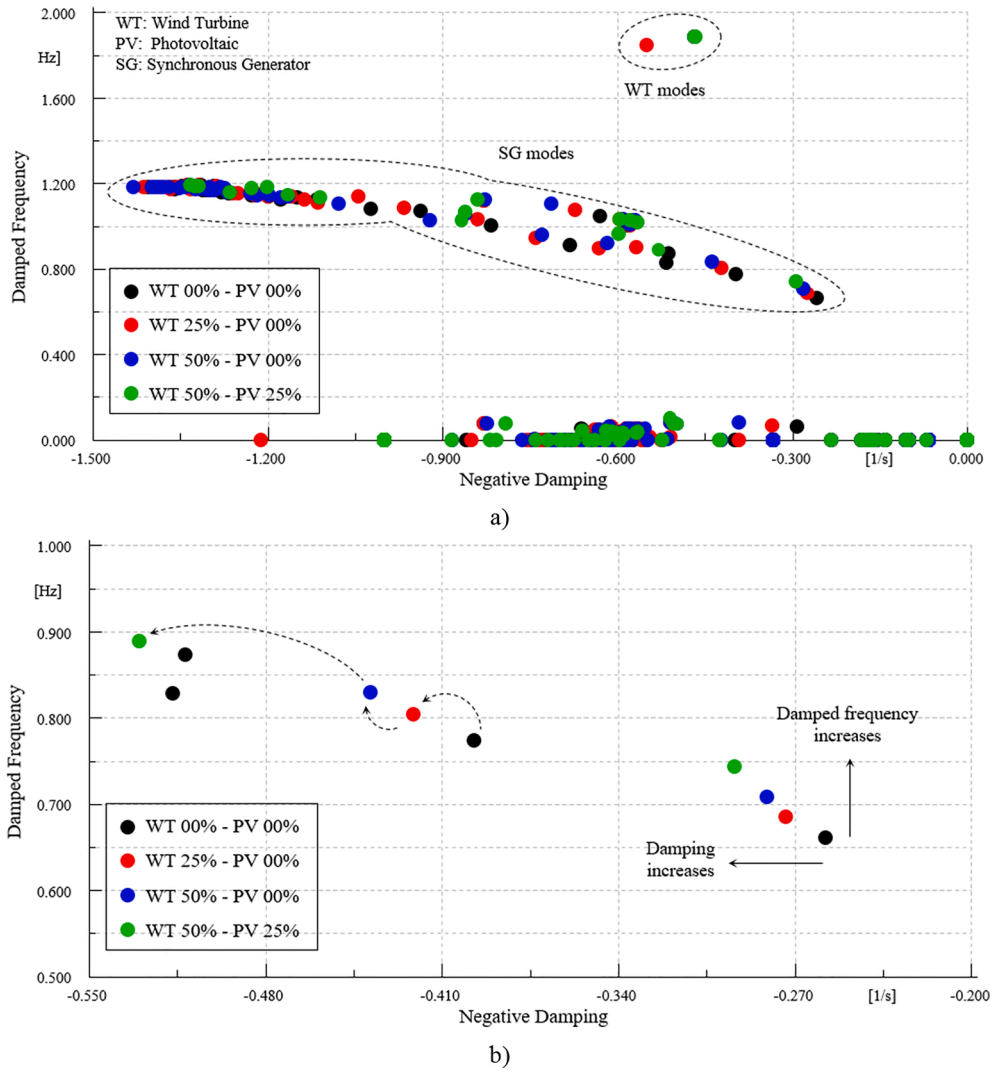

Fig. 13. Effect of WECS and Photovoltaic integration on a) electromechanical modes and b) two slowest electromechanical modes.

all WECS is fed to grid in midpoint. The pitch angle of all WECSs located in zone 19 decreases in order to grow their generated power following the incident. As can be seen from Fig. 10 (a), WTs' speeds mitigate after t = 20 s. This decrement can be visibly observed according to the new equilibrium points of WECSs in right hand side of Fig. 10 (e) at the end of simulation time.

- Second Scenario: Decreasing Wind Speed of All WECSs

In this subsection, the 36-zone GB system frequency response for the scenario of Wind Speed III following the loss of nuclear power located in zone 19 is investigated. The relevant results beside Wind Speed I scenario are illustrated in Figs. 11 and 12. The simulation time interval is 50 s. Moreover, wind speed values are changed at $t = 1$ s for all five regions depicted in Fig. 2 (b), as shown in Fig. 11 (a). Despite Wind Speed II scenario, wind speed of Wind Speed III scenario for all regions of GB network reduces simultaneously. The loss of generator is simulated at $t = 20$ s.

The COI frequency and COI RoCoF of GB network are shown in Fig. 11 (b) and (c), respectively. Furthermore, the inertial power variations of conventional unit as well as WECS are illustrated in Fig. 11 (d) for the initial times of disturbance occurrence. Fig. 11 (e) illustrates conventional and WT turbine power change. The reserve powers of all 5 regions depicted in Fig. 2 (b) are shown in Fig. 11 (f) and (g), including their algebraic summation. The reserve power variations of all four regions where the disturbance did not happen are shown in Fig. 11 (f). In other hand, the corresponding values of Area 03 (Disturbance is occurred in this region) and the power summation of all areas are shown in Fig. 11 (g) for Wind Speed I and Wind Speed III.

Applying the wind speed change of Wind Speed II depicted in Fig. 11 (a) on WECSs leads to output power reduction of WECSs by 2,250 MW. This in turn can abruptly mitigate reserve power of WECSs, as shown in Fig. 11 (f) and (g). As can be seen form right hand side of Fig. 11 (g), the amount of this reduction for the whole network is 225 MW which is quite match to 10 % reserve power of WECSs. This wind speed variation is like loss of wind power leading to system frequency mitigation, as

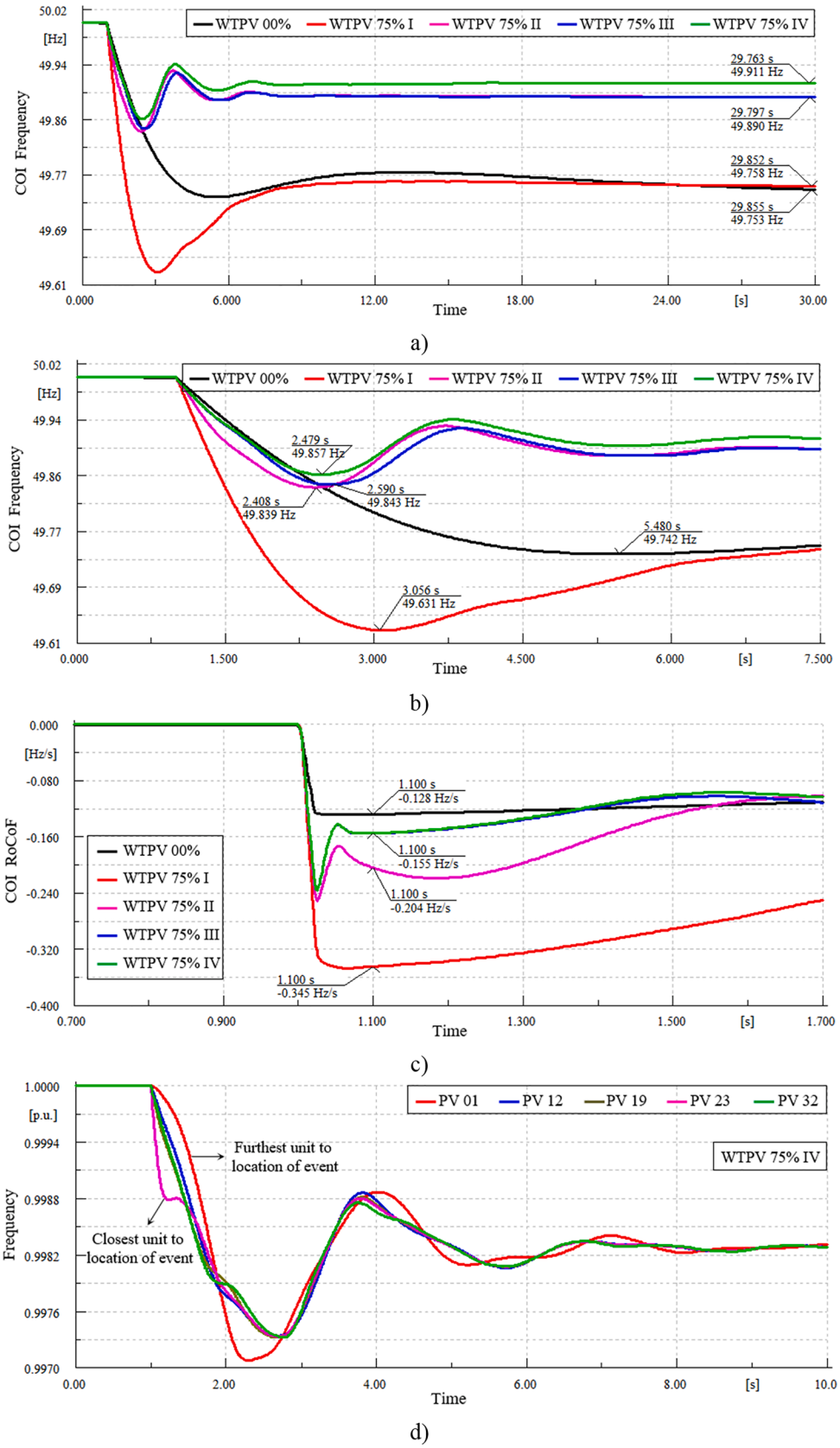

Fig. 14. A) Frequency response b) frequency nadir, c) RoCoF deviations, d) frequency of Pv power plants following the loss of 1700 MW generation in middle of network (Zone 23).

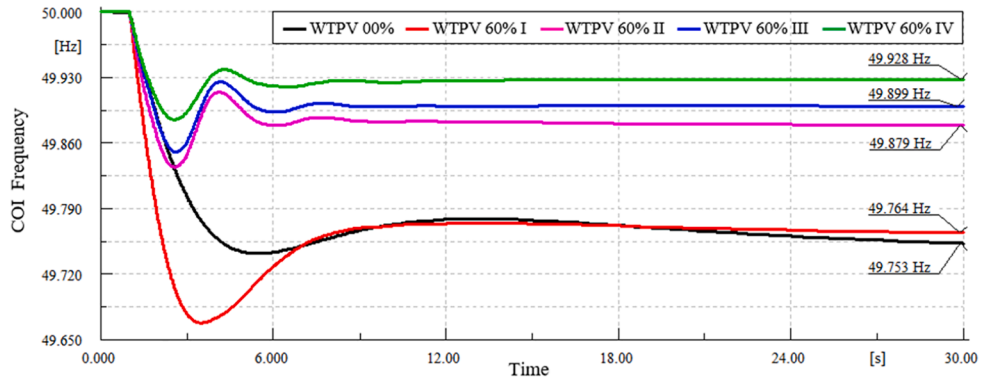

(a)

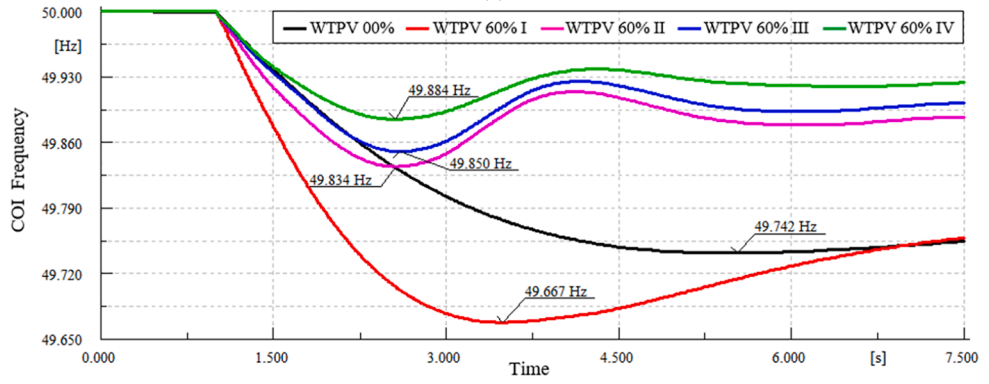

(b)

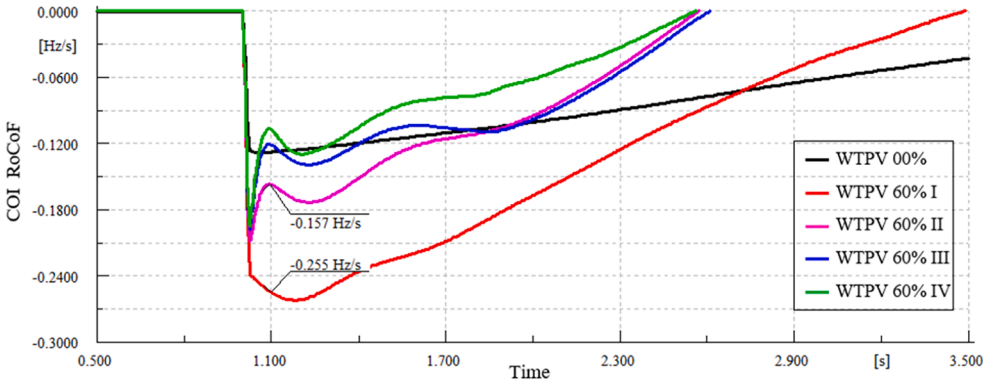

(c)

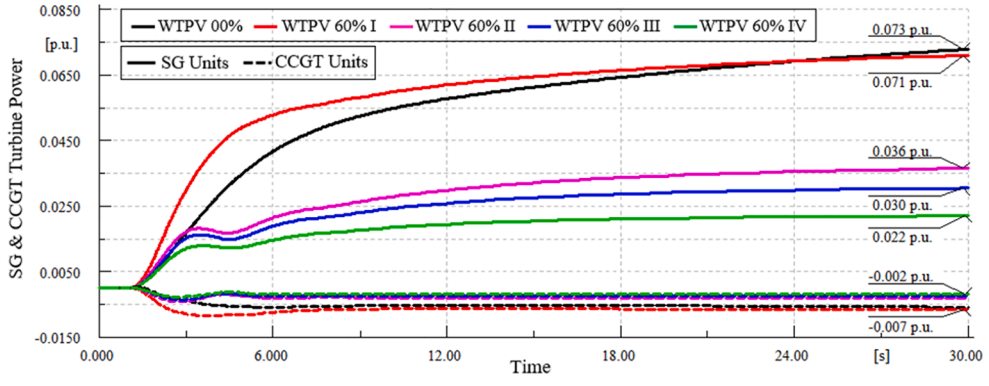

(d)

Fig. 15. (a) Frequency response; (b) Frequency nadir; (c) RoCoF deviations; (d) Turbine power deviations of SGs and CCGTs; and (e) Inertial power changes of SGs and CCGTs; all for loss of 1700 MW generation in middle of network (Zone 23).

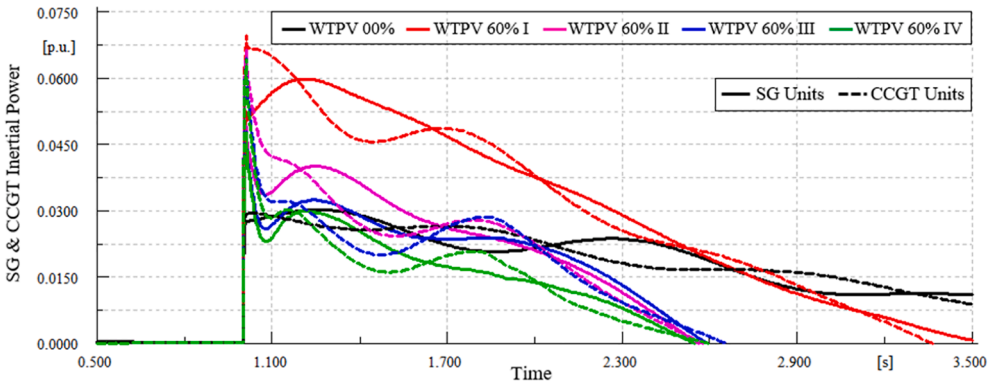

(e)

Fig. 15. (*continued*).

depicted in Fig. 11 (b). Due to this fact, output powers of conventional units and WECSs increase following the event as shown in Fig. 11 (e). As a result, some part of WECSs' reserve power is occupied to compensate WECSs' power reduction in consequent of wind speed changes. The reserve power of WECSs reduces by 52 % from 2,000 MW to 960 MW in $t = 20$ s. This is because the frequency nadir and steady-state frequency deviation in Wind Speed II scenario dropped down by 30 % and 165 % compared to Wind Speed I, respectively. However, the COI RoCoF is equal in both scenarios. Note, the residual reserve power of all WECS is 160 MW at the end of simulation time. The simultaneous wind speed reduction across GB network in Wind Speed III reduces reserve power of all WECSs to zero value within 5 s from the disturbance occurrence time.

In order to accurately investigate the above matter, some quantities related to 5 WECSs specified in Fig. 2 (b), are shown in Fig. 12. The rotor speed, power coefficient and turbine power variations of WECSs are portrayed in Fig. 12 (a) to (c), respectively. Furthermore, pitch angle and power coefficient versus tip speed ratio trajectories are plotted in Fig. 12 (d) for Wind Speed III scenario. The equilibrium points of 5 WECSs on MPPT curves are determined for three times of start point, midpoint (M) and end point (E) which are 0 s, 20 s and 50 s, respectively. It is clear that the sudden decrement of wind speed in $t = 1$ leads to rotor speed buck. This can be justified based on tip speed ratio equality of initial and mid equilibrium points of left hand side of Fig. 12 (e) in Wind Speed III scenario. It is to be notified that five WECSs have dissimilar rotor speed and identical pitch angle in $t = 20$ s. These can be observed in left- and right-hand side of Fig. 12 (d) and (e), respectively. It is noteworthy that 4.5 % out of 10 % of reserve power of all WECS is fed to grid in midpoint. The pitch angle of all WECSs located in zone 19 decreases in order to grow their generated power following the incident. As can be seen from Fig. 12 (a), WTs' speeds mitigate after $t = 20$ s. This decrement can be visibly observed according to the new equilibrium points of WECSs in right hand side of Fig. 12 (e) at the end of simulation time. In addition, it can be clearly seen from Fig. 12 (e) that pitch angle and reserve power of all WECSs reach to zero in Wind Speed III scenario.

4. Illustrative Application: WECS, PV and BESS

In this section, the GB system frequency response is validated following the loss of biomass 23. The main reason for selecting this unit is that its capacity is fixed after integration of PVs and WTs.

4.1. Impact of high integration of RESs on frequency response (Modal analysis & Time-Domain Simulations)

4.1.1. Modal analysis

Once the conventional generating units substitute with the PVs and WTs, some electromechanical modes of the network related to the motion equation of the SG's rotor are replaced with double-mass drive train modes of WTs. The electromechanical modes of 36-zone GB network for four different cases are shown in Fig. 13 (a). They are divided into two groups of SG modes and WT modes which are representative of dynamic behavior of the SG's rotor and WTs. The frequency and damping of SG modes are approximately fixed or slightly increased in consequence of increasing PVs and WTs penetration levels.

In order to accurately observe and investigate the effect of growing renewable energy sources penetration levels on electromechanical modes in the 36-zone GB network, two slowest modes are shown in Fig. 13 (b) for different scenarios. It is clear-cut that damping and frequency of these two modes are increased following the RESs' penetration levels increment. This is due to the fact that the AVRs of CCGTs are removed after CCGTs replacement procedure and their negative influence on electromechanical modes i.e. damping reduction mitigates and their damping increases.

4.1.2. Time-Domain simulation

The biomass unit located in zone 23 with the capacity of 1,700 MW is abruptly disconnected from the grid. The simulation results are shown in Fig. 14 for two scenarios of WTPV 75 % and WTPV 00 %. In order to investigate the dynamic performance of PVs and WTs, the WTPV 75 % scenario is divided into four sub-scenarios. In WTPV 75 % I, the inertia emulator and PCO are deactivated for all PVs and WECSs. In scenario of WTPV 75 % II, the WTs are equipped with reserve and inertial powers. It is to be pointed out that the PVs don't have these abilities. In WTPV 75 % III scenario, the PV units are equipped with inertia emulators as well. Finally, the reserve power is considered for all PVs in WTPV 75 % IV scenario.

According to Fig. 14, it is clearly observed that the RoCoF increases expressively once renewable energy sources don't have inertial power feature (in WTPV 75 % I) compared to the scenario of non-renewable energy sources (in WTPV 00 %). This can lead to frequency nadir increment. It is due to the fact that they don't contribute to the inertial frequency regulation of GB system. On the other hand, in WTPV 75 % II

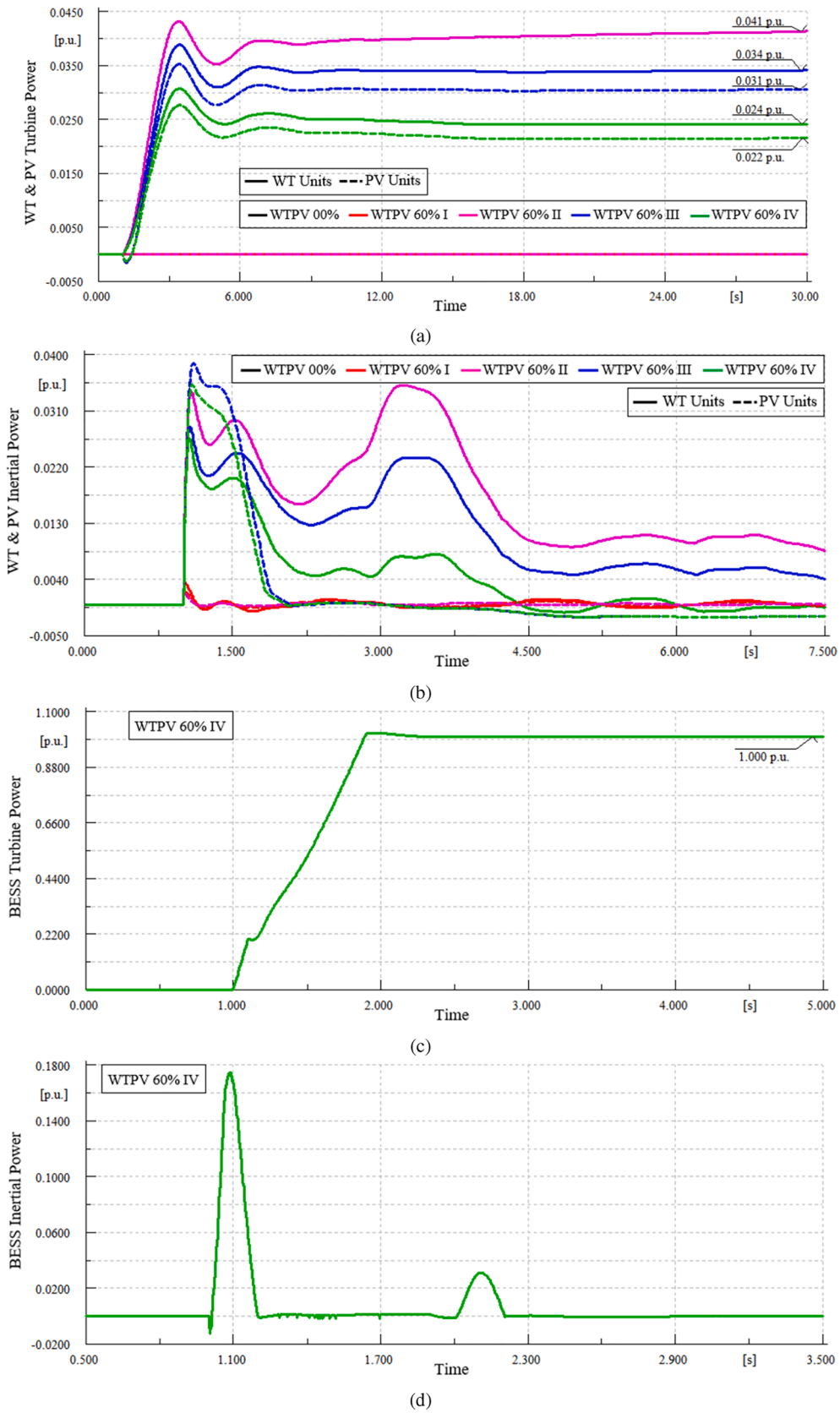

Fig. 16. (a) Turbine power changes of WT and PV units; (b) Inertial power changes of WT and PV units; (c) Turbine power changes of BESS unit; (d) Inertial power changes of BESS unit; (e) Frequency nadir flag of BESS 23; and (f) DC link voltage of BESS 23; all for loss of 1700 MW generation in middle of network (Zone 23).

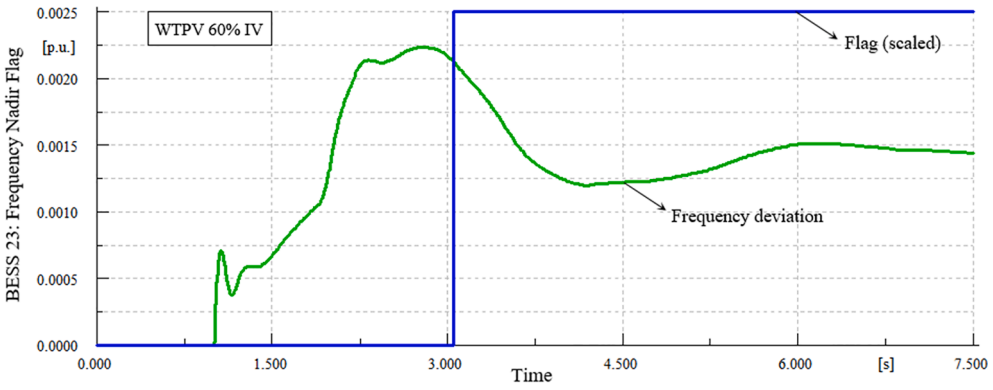

(e)

Fig. 16. (*continued*).

and (WTPV 75 % III and IV) scenarios with respective inertial response releasement of WTs and (both WTs and PVs), the RoCoF and the frequency nadir are considerably decreased.

In order to precisely investigate the dynamic performance of the PV systems in response of generation trip, the variables associated with five PV units from different locations of GB networks are shown in Fig. 14. (d). In this figure, frequency measured in corresponding locations is portrayed. The maximum and minimum RoCoF values are respectively pertinent to the PV 23 and PV 01 which is quite matched with their electrical distance to incident.

4.2. Impact of BESSs' frequency response

To have a meaningful observation in comparison with the results presented in section 3, the same RESs is chosen. The effect of BESS with nominal values of 500 MVA and 50 MWh located in zone 23 on GB system frequency response is investigated hereinafter. The biomass unit located in zone 23 with the capacity of 1700 MW is abruptly disconnected from the grid. The simulation results are shown in Fig. 15 and Fig. 16 for two scenarios of WTPV 60 % and WTPV 00 %. In order to investigate the dynamic performance of the PVs, WTs and the BESS, the WTPV 60 % scenario is divided into four sub-scenarios. In WTPV 60 % I, the inertia emulator and PCO are deactivated for all PVs and WECSs. In scenario of WTPV 60 % II, the WTs are equipped with reserve and inertial powers. It is to be pointed out that the PVs don't have these abilities. In WTPV 60 % III scenario, the PV units are equipped with inertia emulator and reserve power as well. Finally, the proposed BESS model is considered in WTPV 60 % IV scenario. The inertial and reserve powers of WTs and PVs are restricted to 0.1p.u. The inertial and reserve ramp rates of these units are 1p.u. per second and 0.1p.u. per second, correspondingly. In contrast, the parameters of inertia emulator of the 'BESS 23′ are similar to WTs and PVs, however, its maximum reserve power is assumed to be 1p.u and it can be increased by 2p.u. per second. The droop coefficient of all units is 5 %, however, this is selected as 0.05 % for the BESS.

According to Fig. 15 (a) to (c), it is clearly observed that the COI frequency criteria like RoCoF and frequency nadir are significantly aggravated in WTPV 60 % I compared to WTPV 00 % due to considerable decrement of system inertial power. However, steady-state frequency deviation is identical. This is because that the inertia drops in WTPV 60 % results in steady-state frequency deviation increment following the first few seconds of disturbance occurrence so that the SGs can generate much more power and make the frequency closer to that of the WTPV 00 % scenario, as shown in Fig. 15 (d). In other hand, according to Fig. 15 (e), the SGs and CCGTs generate greater inertial power, however, RoCoF is deteriorated as the inertial power is in p.u. Moreover, the base power is also the algebraic summation of installed generating power of each scenario. Thus, the inertial power WTPV 00 % is greater than WTPV 60 % I.

In other hand, in WTPV 60 % II where WTs are participated in primary frequency support beside the SGs, the COI frequency criteria in terms of RoCoF is slightly deteriorated with respect to WTPV 00 % scenario due to supplying of 20 % of load demand by PVs which are not equipped with inertia emulators. However, the frequency nadir and steady-state frequency deviation are enhanced due to higher power ramp rate of WTs compared to SGs in the first 5 s following the incident, as shown in Fig. 16 (a). In other hand, the inertial power produced by the SGs in WTPV 60 % II us located between those of scenarios WTPV 00 % and WTPV 60 % I (See Fig. 16 (e)). In WTPV 60 % III scenario where PVs are equipped to primary frequency support like SGs and WTs, the COI frequency in terms of RoCoF, frequency nadir, steady-state frequency deviation are slightly enhanced as compared to WTPV 60 % II due to primary frequency support increment. Based on Fig. 16 (a) to (c), this leads to enhancement of RoCoF with respect to WTPV 60 % II. Further, this RoCoF becomes equal to that of WTPV 00 % scenario. Additionally, it is to be noted that frequency support burden on the WTs in supplying the system power lost decreases as PVs are equipped with inertia emulators and primary frequency control, as depicted in Fig. 16 (a) and (b).

Finally, in last scenario i.e. WTPV 60 % IV where a BESS is installed in zone 23, the system frequency response is considerably enhanced in this scenario so that the RoCoF is almost identical to WTPV 00 %. In other hand, frequency nadir and steady-state frequency deviation are respectively improved by 23 % and 28 % respectively in this scenario in comparison with WTPV 60 % III due to supplying power by the BESS, as shown in Fig, 16 (c) and 16 (d). The main meaning of turbine power in Fig. 16 (c) is output power of the VRB battery in the BESS unit. It is notable that generated power by the BESS is increased to its nominal amount i.e. 500 MW within 1 s. Moreover, the ramp up rate of the BESS is approximately half of its upper limit. This is due to the fact that the generation lost is not huge so that the ramp up rate of its reference power in the PCO of the 'BESS 23′ reaches to its maximum limit. The steady state frequency deviation (i.e. 28 %) is almost identical to the BESS

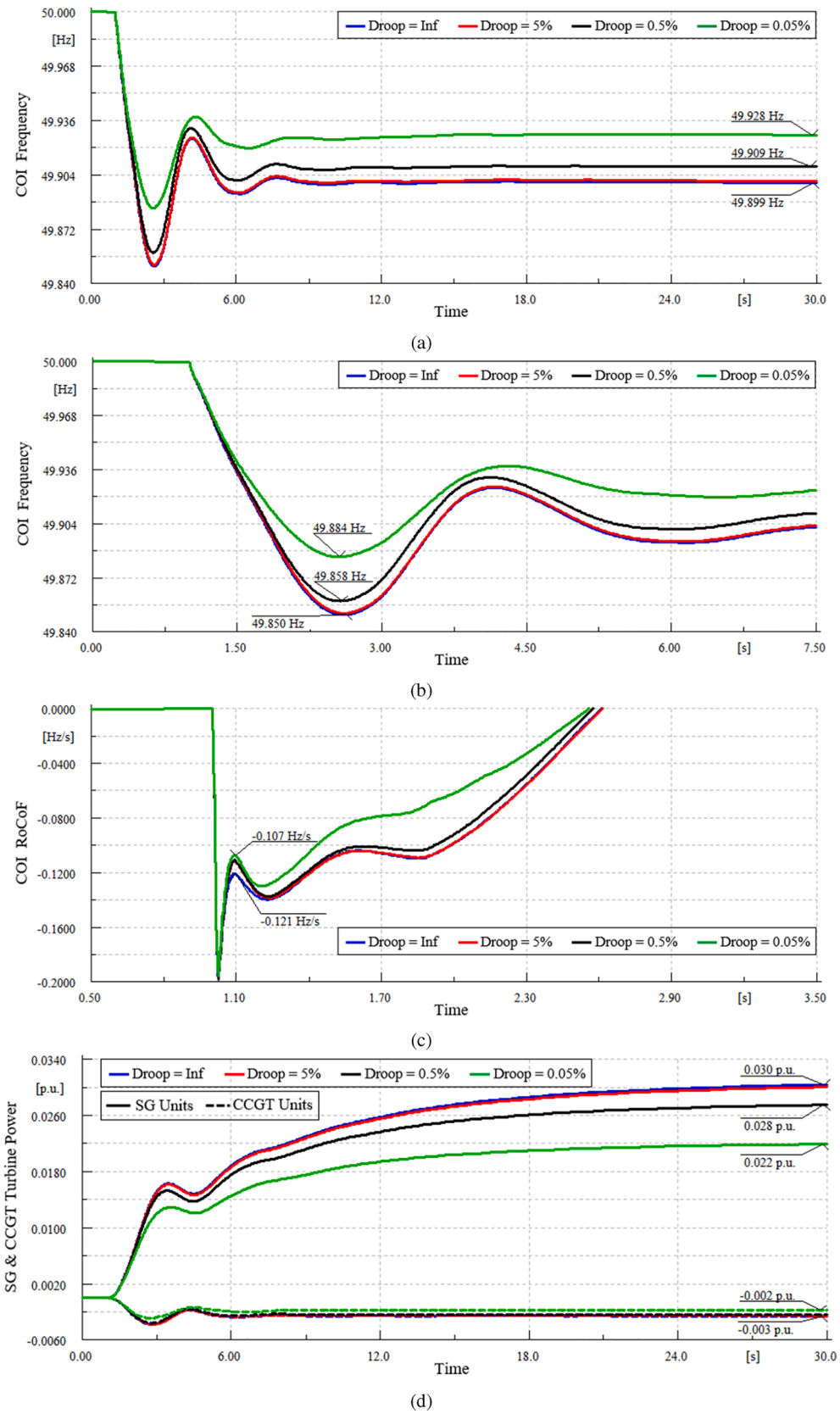

Fig. 17. (a) Frequency response; (b) Frequency nadir; (c) RoCoF deviations; (d) Turbine power changes of SG and CCGT units; (e) Inertial power changes of SG and CCGT units; all for loss of 1700 MW generation in middle of network for different BESS droop (Zone 23).

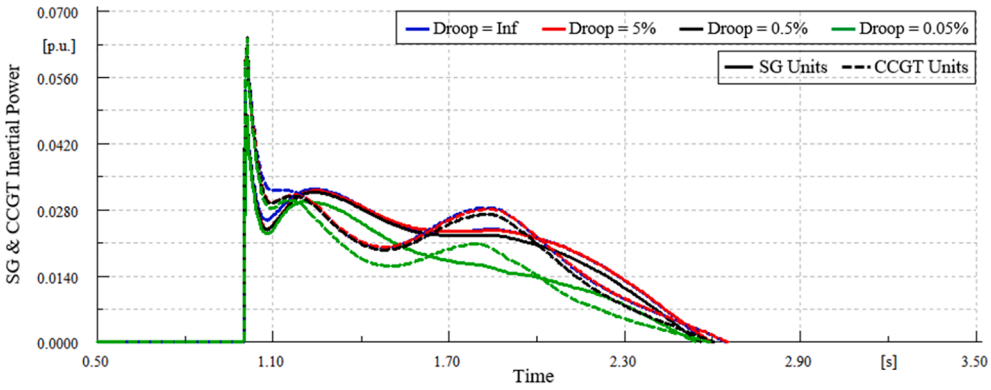

(e)

Fig. 17. (*continued*).

contribution in supplying of generation lost, that is, 29 %. In the last scenario, according to Fig. 15 (d) and Fig. 16 (a), the system frequency support burden on the SGs, WTs and PVs are also mitigated. Based on Fig. 16 (e) and (f), the dc link voltage recovery of the 'BESS 23′ is started at appropriate moment. Finally, the generating of power equal to 500 MW for 28 s by the 'BESS 23′ reduces its SOC by 6 %.

4.3. Impact of BESS droop

The influence of droop parameter (*R*) of the Primary Controller of the 'BESS 23′ on GB system frequency response is analyzed. In this context, the results of four scenarios following loss of biomass unit located in zone 23 are shown in Fig. 17 and Fig. 18. The first scenario highlighted with blue traces is identical to WTPV 60 % III in the previous section. In this scenario, all SGs, WTs and PVs have primary frequency support. It is noteworthy that selecting an infinite droop for the BESS means it is deactivated. The fourth scenario highlighted with green traces is identical to WTPV 60 % IV in previous section in which the droop amount of the 'BESS 23′ is 0.05 %. The third scenario is highlighted with black traces is similar to fourth scenario, except that the droop parameter for the 'BESS 23′ is set to 0.5 %. Finally, in second scenario which is highlighted by red traces, is similar to third scenario except that the droop parameter of the 'BESS 23′ is considered to be 5 %. As can be seen from simulation results, the network frequency is just slightly changed if the droop parameter of the 'BESS 23′ is equal to other units, compared to when it is deactivated. This change is, as a result of increased primary frequency support of network with the 'BESS 23′ installation, in order to make the system frequency closer to its nominal one. In other hand, in third scenario where the droop parameter of the BESS 23 is one-tenth of other units, the power output of this storage unit is increased from 0.04p.u. to 0.34p.u. This leads to 10 % and 5 % enhancement of steady-state frequency deviation and frequency nadir respectively with respect to second scenario. Finally, while the droop parameter of the BESS 23 is considered to be one-hundredth of other units in fourth scenario, about 30 % of generation lost is supplied by this energy storage unit. This results in 21 % and 18 % improvement of steady-state frequency deviation and frequency nadir respectively in comparison of third scenario. However, as can be observed from Fig. 17 (d), the mitigation of droop parameter of the BESS or increasing the sensitivity of this unit in terms of system frequency variation, can lead to inertial power reduction of dc link capacitor. This can consequently result in a lower change of dc link voltage amplitude, as shown in Fig. 17 (f). The main reason behind this fact can be the double ramp up rate of the BESS generated power with respect to ramp up rate of inertial power captured from dc link capacitor of the BESS 23. Additionally, it is quite clear that while the droop parameter of the BESS is reduced and its sensitivity to system frequency increased, more energy will be extracted from the battery so that its SOC will be correspondingly mitigated.

4.4. Impact of BESS installation location

In this subsection, the influence of the BESS installation location on its primary frequency support and GB system frequency response is evaluated. In this regard, four discrepant sorts relating to four installation locations of the BESS with 500 MVA and 50 MWH (one in the most bottom part of network, one near to the condensed load, one near to the top area and the last one near to the disturbance location at zone 23) are defined. It is to be noticed that for each of these four scenarios, just one BESS is activated. The parameters tuning is identical to that of last scenarios presented in previous subsections. Furthermore, the droop coefficients of all BESS units are equal to 0.05 %.

The simulation results of the above-mentioned scenarios following the loss of biomass unit 23 are shown in Fig. 19. As can be seen from Fig. 19 (a), the system COI frequency for all the BESSs located in different locations of the grid is almost similar. According to Fig. 19 (b) and (c), when the BESS is closer to the disturbance location, i.e. third scenario, the frequency nadir and RoCoF are improved. In contrast, in the first scenario where the BESS is installed in a farthest place from incident that is, zone 1 the above-mentioned frequency criteria are deteriorated. For the sake of comparison, these two quantities are enhanced by 2.5 % and 10 % respectively in scenario 3 (best case) compared to the first scenario (Worst case). Following the third scenario, the second and fourth ones are the best case in terms of frequency nadir when the BESS is in zone 8 and 30, respectively. However, the steady-state frequency deviation in case of installing the BESS in zone 8 is lower than installing it nearer to the disturbance, i.e. zone 23. Additionally, this justification can be also followed for the generated power shown in Fig. 19 (d) to (g).

The simulation results related to the BESS are shown in Fig. 20 (a) to (f). The influence of the installing BESS in different parts of the network is clearly investigated following the disturbance occurrence. As can be seen from Fig. 20 (a), the powers generated by the BESS located in zone

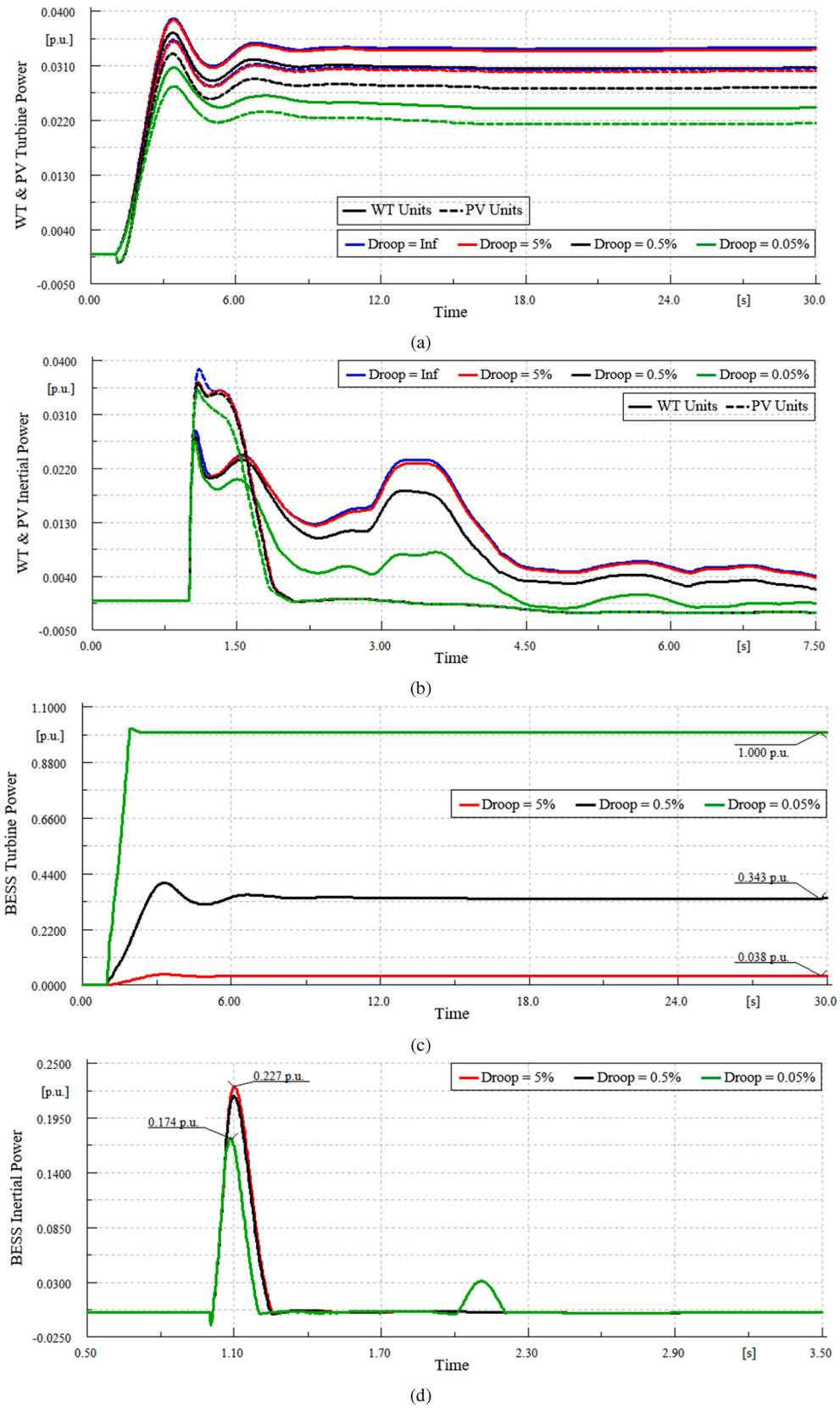

Fig. 18. (a) Turbine power changes of WT and PV units; (b) Inertial power changes of WT and PV units; (c) Turbine power changes of BESS; (d) Inertial power changes of BESS unit; (e) Frequency nadir flag of BESS 23; and (f) DC link voltage of BESS 23; all for loss of 1700 MW generation in middle of network for different BESS droop (Zone 23).

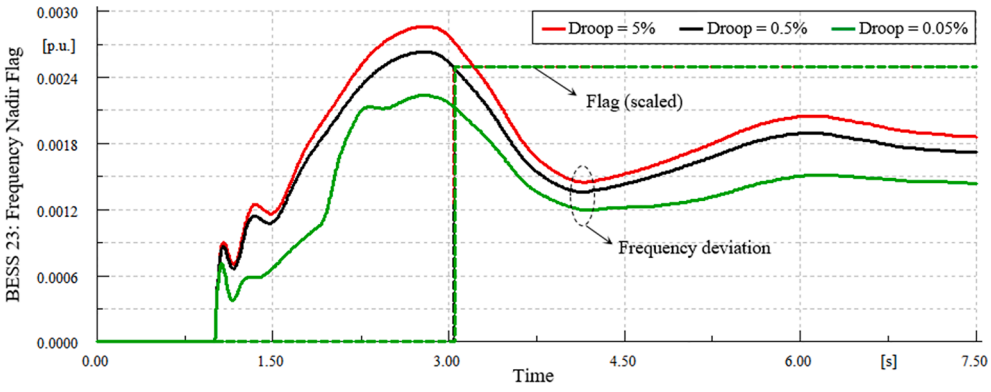

(e)

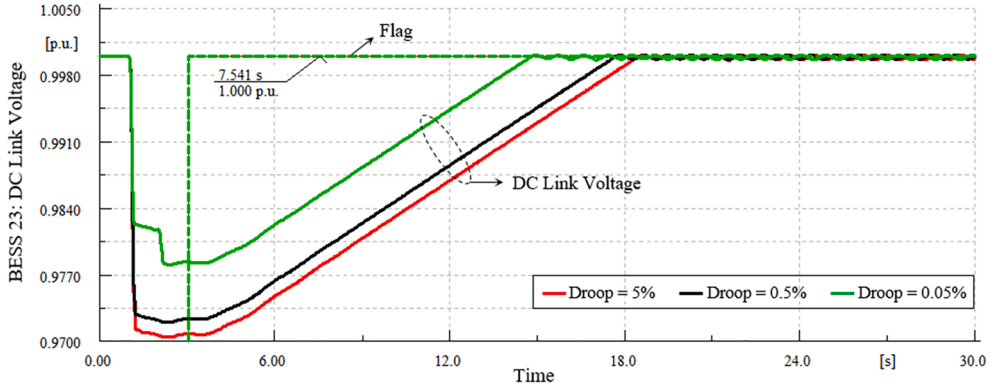

(f)

Fig. 18. (*continued*).

23 and 1 are increased faster and slower compared to others, respectively. In addition, it is observed that when the BESS is placed near to the event, the ramp up rate of power is limited to the 'Rate Limiter' block in PCO controller for the first 100 ms of disturbance. This can be justified based on fast frequency reduction in Fig. 20 (c). The effect of BESS location on inertial power of BESS is presented in Fig. 20 (b). It is observed that zones 23, 30, 8 and 1 have the lowest frequency distance with the event location, respectively. The frequency nadir time is similar for all scenarios. The way of changing dc link voltage amplitude of the BESS units is shown in Fig. 20 (d). The voltage drop is conducted in two stages. The voltage drop amount is proportional to the area under the inertial power curve, as shown in Fig. 20 (b). To be precise, it is to be noted that the voltage drop square is proportional to inertial energy (the area under the inertial power curve). In the time interval of 1–1.7 s, scenarios 3, 4, 2 and 1 have the highest inertial energy and highest voltage drop, respectively. This order is changed to scenarios 1, 4, 2 and 3 for the time interval 2.5–3 s. The SOC of all BESSs is portrayed in Fig. 20 (e). The lowest and highest amounts of SOC are associated with scenarios 3 and 1, respectively. This can be also induced by comparing the area under battery power curve in Fig. 20 (a). Finally, the voltage and current variation of the VRB batteries are shown in Fig. 20 (f) following the incident. Due to less amount of voltage amplitude change, the current change is identical to power change as shown in Fig. 20 (a).

5. Conclusions

In this study, the WECS, PV and BESS are modelled and integrated into the Great Britain (GB) power system, which is reduced to 36-zone system. These models are generically developed based on the literature review and are not intended to be representative of specific generation connections within the NGESO GB master system. The simulations result of WECSs' integration are provided for three main sub-scenarios i.e., WECSs without inertial emulator and reserve power, only inertial emulator and with both inertial emulator and reserve power. A comparison between the non-WECSs and WECSs without inertial power and reserve power clearly shows that both RoCoF and frequency nadir are deteriorated in case of WECSs without inertial power and reserve power. Furthermore, it can be deduced that the steady-state frequency deviation in these two scenarios is almost identical. However, conventional units generate more power in WT 00 % scenario compared to WT 25 %. In case that WECSs can provide inertial power, the system RoCoF is improved, however, it is still worse than WT 00 %. Moreover, it is observed that inertial power generated by WECSs has a slight influence (below 5 %) on frequency nadir improvement. By taking the WT operating characteristics and conditions into account, the available inertial power and reserve power are utilized in a rational manner, and therefore the system frequency stability in terms of frequency nadir and steady-state frequency deviation compared to WT 00 %, WT 25 % I and WT 25 % II is enhanced. However, the system RoCoF in WT 25 % scenario is still worse than WT 00 %. The reason is that the increment rate of WTs' inertial power is restricted to 1p.u. per second. The influence of inertial power increment rate on system frequency response is analyzed. The COI RoCoF is reduced with increasing the inertial power rate increment. The wind speed variations impact on GB

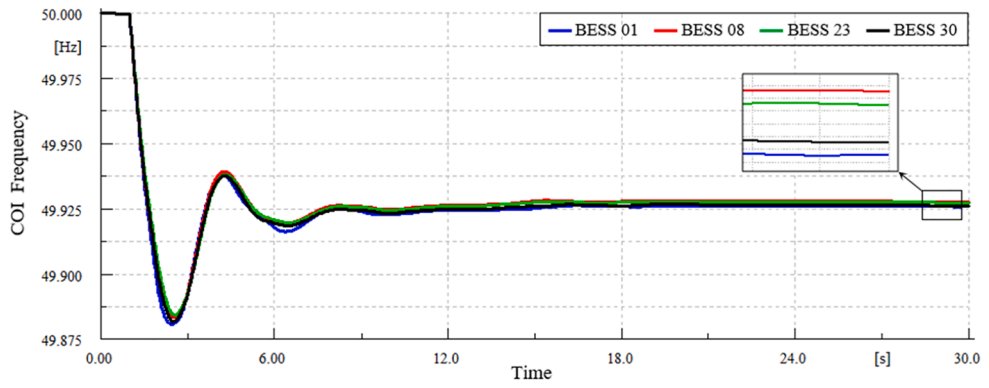

(a)

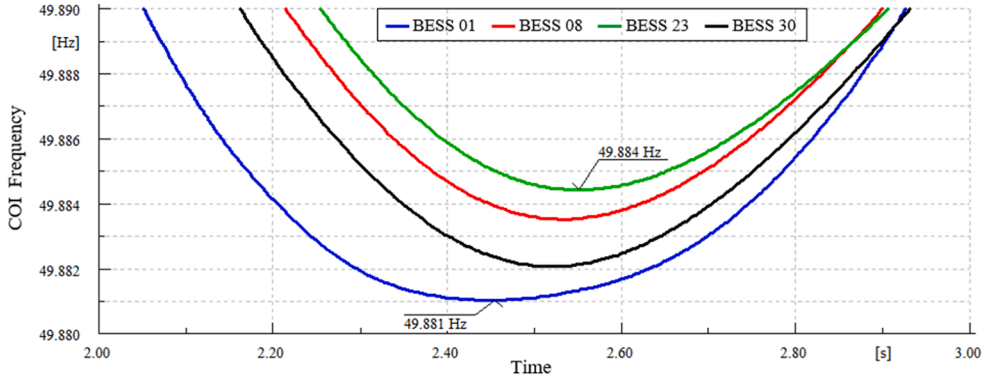

(b)

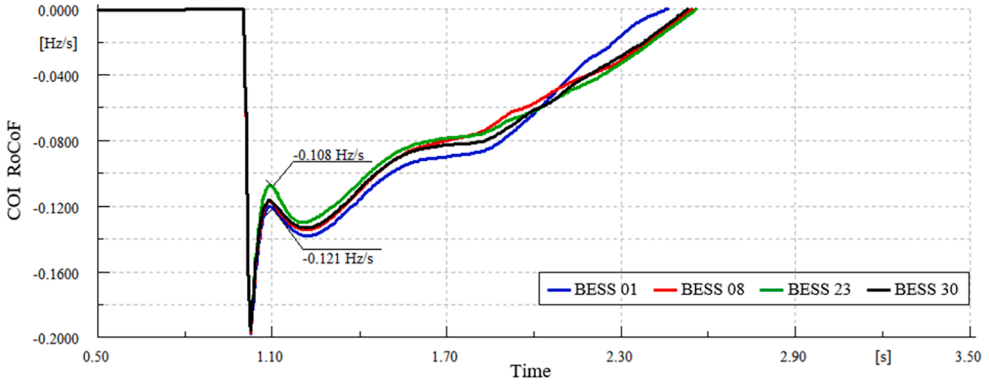

(c)

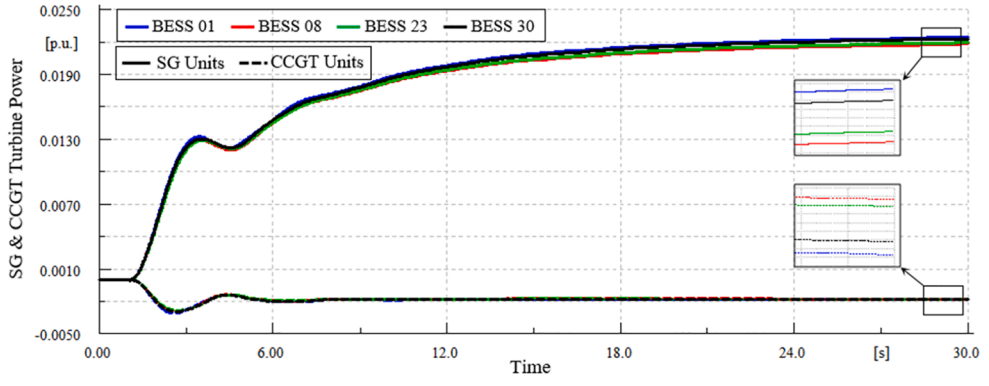

(d)

Fig. 19. Frequency response; (b) Frequency nadir; (c) RoCoF deviations; (d) Turbine power changes of SG and CCGT units; (e) Inertial power changes of SG and CCGT units; (f) Turbine power changes of WT and PV units; and (g) Inertial power changes of WT and PV units; all for loss of 1700 MW generation in middle of network for different BESS droop (Zone 23).

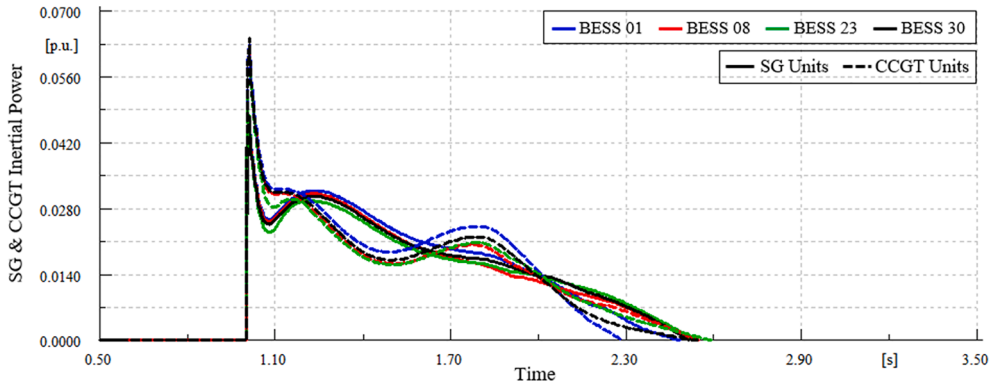

(e)

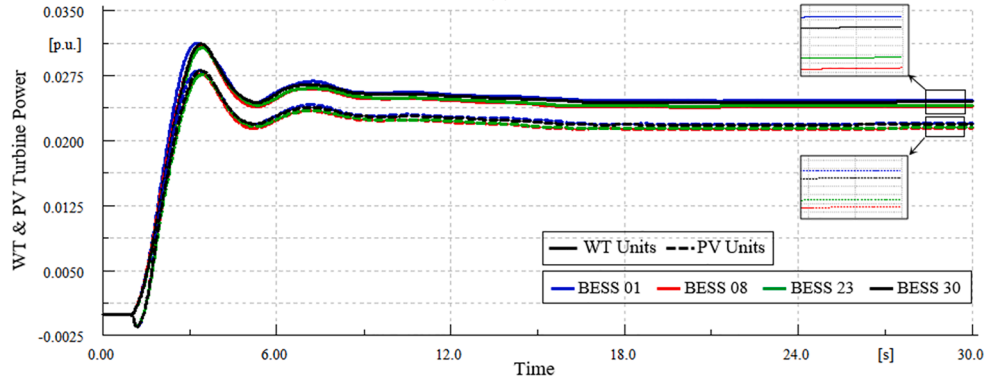

(f)

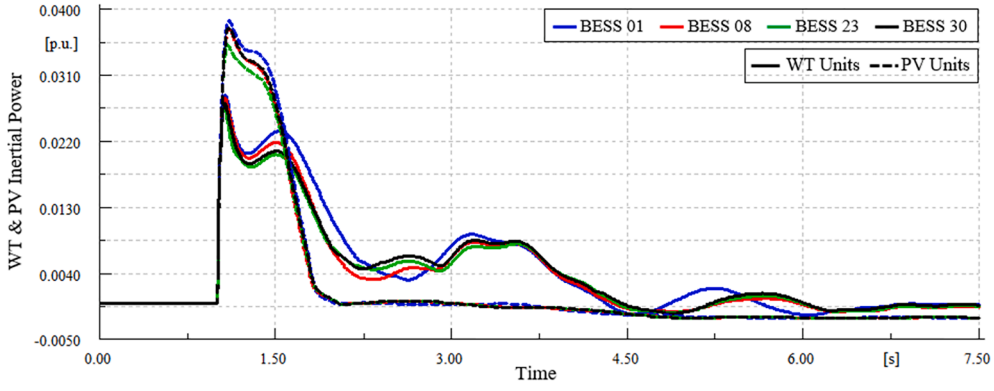

(g)

Fig. 19. (*continued*).

system frequency response under 50 % penetration of wind power is investigated. It is observed that while the average value of wind speed variations per each MW wind power capacity installation is negative, the reserve power of WECSs has dropped down. As a result, once a generator is disconnected, the frequency nadir and steady-state frequency deviation deteriorate compared to the fixed wind speed case. In addition, when the wind speed reduces in such a way that available reserve power of all WECSs before the event is less than half a generation lost, this reserve power will be dropped down to zero after the event. This half a power can be inferred according to 50 % penetration level of WECSs and equal value of R i.e. 0.05 in PCO of WECSs and conventional units. However, it is clearly shown that reserve power changes of WECSs caused by wind speed variation have a minor effect on system RoCoF. The dynamic performance of the 36-zone model under high integration of RESs i.e. 75 % is investigated. It is observed that the PV system with reserve and inertial frequency support capabilities can enhance frequency stability criteria like RoCoF, frequency nadir and steady-state frequency deviation.

Furthermore, the dynamic performance of the proposed BESS system is investigated. It is observed that the BESS system with reserve and inertial frequency support capabilities can enhance frequency stability criteria like RoCoF, frequency nadir and steady-state frequency deviation. However, this enhancement is proportional to the ratio of the BESS nominal power and power disturbance size. In addition, the primary

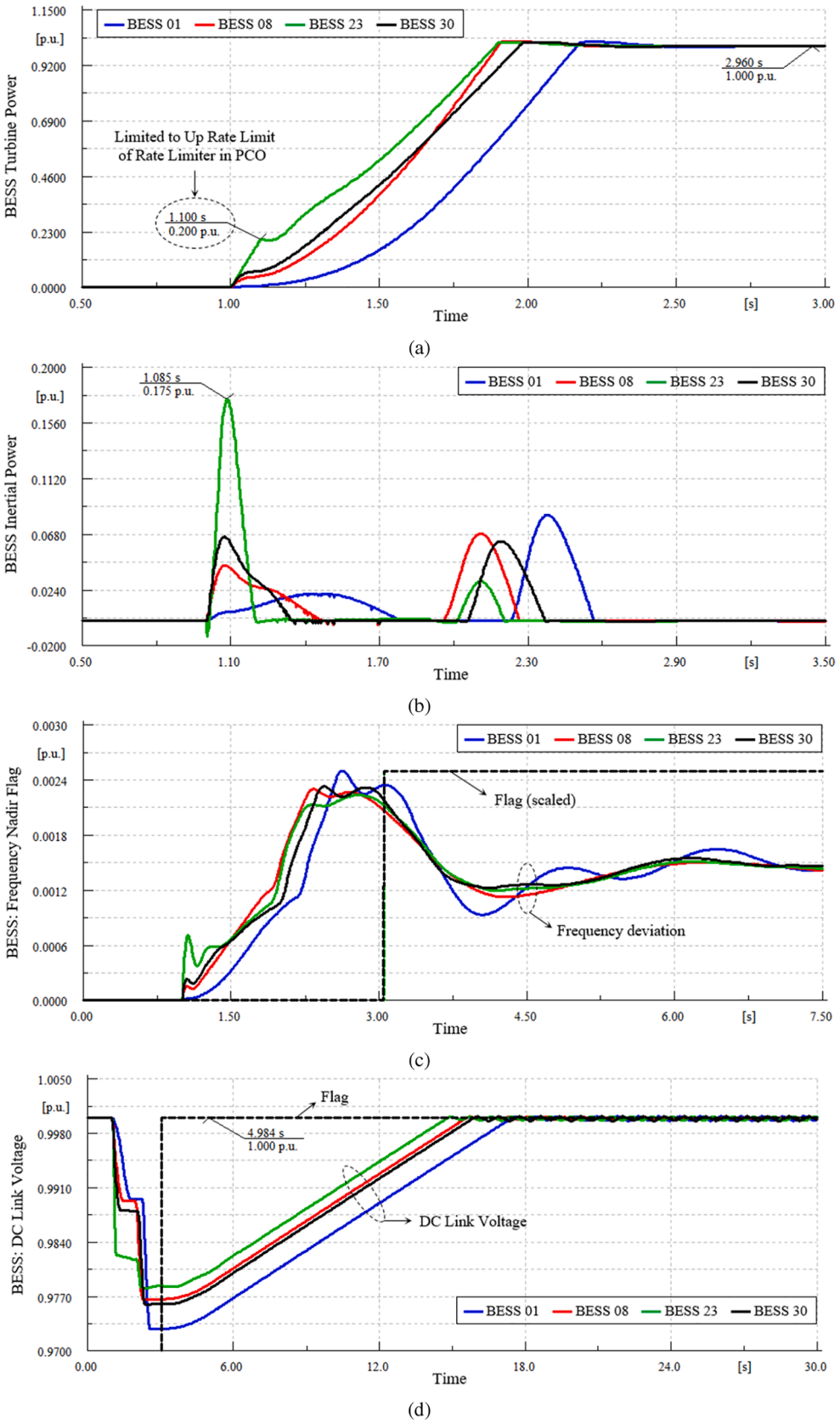

Fig. 20. (a) Turbine power changes of BESS units; (b) Inertial power changes of BESS units; (c) Frequency nadir flag of BESS units; (d) DC link voltage of BESS units; (e) State of charge of BESS units; and (f) Battery current and voltage of BESS 23; all with loss of 1700 MW generation in middle of network for different BESS location (Zone 23).

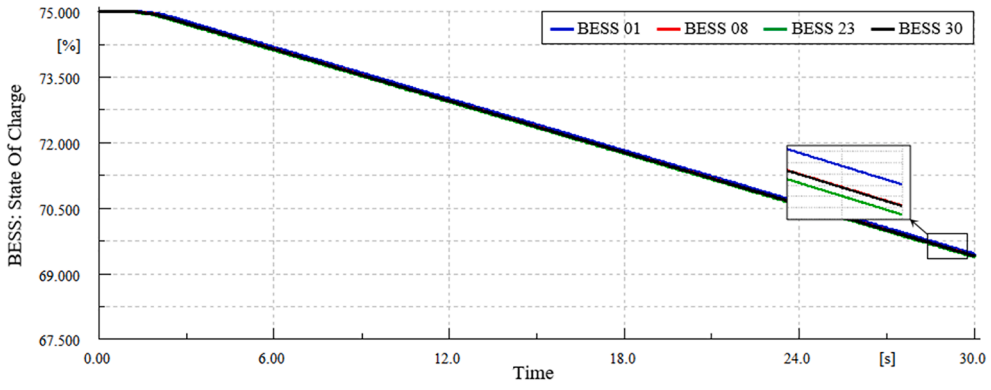

(e)

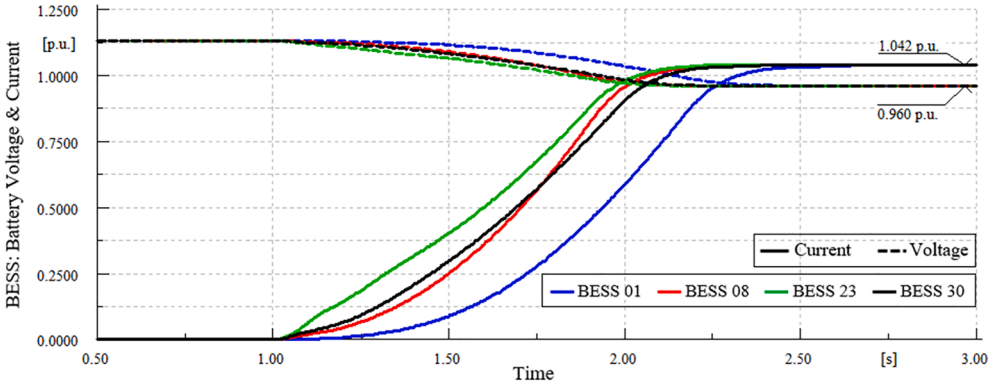

(f)

Fig. 20. (*continued*).

frequency support burden on conventional units and or WTs and PVs is mitigated accordingly. It is also deduced that closeness of the BESS unit to the disturbance location has considerable impact on its inertial frequency response so that the nearer units inject more inertial power to the grid. Furthermore, the BESS location hasn't considerable impact on primary frequency support, however, the droop parameter has significant effect and needs to be selected appropriately.

CRediT authorship contribution statement

Rasoul Azizipanah-Abarghooee: Conceptualization, Methodology, Software, Validation, Formal analysis, Investigation, Resources, Data curation, Writing – original draft, Writing – review & editing, Supervision, Project administration. **Mostafa Malekpour:** Methodology, Software, Formal analysis, Investigation, Data curation, Writing – original draft, Writing – review & editing, Visualization. **Mazaher Karimi:** Methodology, Validation, Investigation, Writing – original draft, Visualization, Funding acquisition. **Vladimir Terzija:** Conceptualization, Resources, Data curation, Writing – review & editing, Supervision, Project administration.

Declaration of competing interest

The authors declare that they have no known competing financial interests or personal relationships that could have appeared to influence the work reported in this paper.

Data availability

The data that has been used is confidential.

Acknowledgment

The authors would like to thank National Grid ESO for providing the 36-zone GB power system reduction data as well as EFCC team for their insightful comments on the paper.

References

[1] IEC White Paper, "Grid integration of large-capacity renewable energy sources and use of large-capacity electrical energy storage," Int. Electrotech. Comm., Geneva, Switzerland, Tech. Rep., 2012.
[2] Margaris D, Papathanassiou SA, Hatziargyriou ND, Hansen AD, Sorensen P. Frequency control in autonomous power systems with high wind power penetration. IEEE Trans Sustain Energy Apr. 2012;3(2):189–99.
[3] Conroy JF, Watson R. Frequency response capability of full converter wind turbine generators in comparison to conventional generation. IEEE Trans Power Syst May 2008;23(2):649–56.
[4] Morren J, Pierik J, De Haan SW. Inertial response of variable speed wind turbines. Electric Power Syst Res Jul. 2006;76(11):980–7.
[5] Nanou SI, Patsakis GN, Papathanassiou SA. Assessment of communication-independent grid code compatibility solutions for VSC–HVDC connected offshore wind farms. Electric Power Syst Res Apr. 2015;121:38–51.
[6] Arani MF, El-Saadany EF. Implementing virtual inertia in DFIG-based wind power generation. IEEE Trans Power Syst May 2013;28(2):1373–84.
[7] Delille G, Francois B, Malarange G. Dynamic frequency control support by energy storage to reduce the impact of wind and solar generation on isolated power system's inertia. IEEE Trans Sustain Energy Oct. 2012;3(4):931–9.
[8] Datta M, Senjyu T, Yona A, Funabashi T, Kim CH. A frequency-control approach by photovoltaic generator in a PV–diesel hybrid power system. IEEE Trans Energy Convers Jun. 2011;26(2):559–71.
[9] Kakimoto N, Takayama S, Satoh H, Nakamura K. Power modulation of photovoltaic generator for frequency control of power system. IEEE Trans Energy Convers Dec. 2009;24(4):943–9.
[10] Bao W, Ding L, Liu Z, Zhu G, Kheshti M, Wu Q, et al. Analytically derived fixed termination time for stepwise inertial control of wind turbines—Part I: Analytical derivation. Int J Electric Power Energy Syst Oct. 2020;121:106120.
[11] Guo Y, Bao W, Ding L, Liu Z, Kheshti M, Wu Q, et al. Analytically derived fixed termination time for stepwise inertial control of wind turbines—Part II: Application strategy. Int J Electric Power Energy Syst Oct. 2020;121:106106.

[12] Keung P-K, Li P, Banakar H, Ooi BT. Kinetic energy of wind-turbine generators for system frequency support. IEEE Trans Power Syst Feb. 2009;24(1):279–87.
[13] De Almeida RG, Peças Lopes JA. Participation of doubly fed induction wind generators in system frequency regulation. IEEE Trans Power Syst, Aug 2007;22(3):944–50.
[14] Driesen J, Visscher K. "Virtual synchronous generators", in Proc. Pittsburgh, PA: IEEE PES General Meeting; Jul. 2008.
[15] Kushwaha P, Prakash V, Bhakar R, Yaragatti UR. Synthetic inertia and frequency support assessment from renewable plants in low carbon grids. Electr Power Sys Res Aug. 2022;209:107977.
[16] Prakash V, Kushwaha P, Sharma KC, Bhakar R. Frequency response support assessment from uncertain wind generation. Int J Electric Power Energy Syst Jan. 2022;134:107465.
[17] Prakash V, Pandzic H. Fast frequency control service provision from active neighborhoods: Opportunities and challenges. Electr Power Sys Res Apr. 2023;217:109161.
[18] Loukarakis E, Margaris I, Moutis P. "Frequency control support and participation methods provided by wind generation," *In: Electrical Power & Energy Conference (EPEC)*, 2009 IEEE 2009 Oct 22 (pp. 1-6). IEEE.
[19] Mercier P, Cherkaoui R, Oudalov A. Optimizing a Battery Energy Storage System for Frequency Control Application in an Isolated Power System. IEEE Trans Power Syst 2009;24(3):1469–77.
[20] Swierczynski M, Stroe DI, Stan AI, Teodorescu R, Sauer DU. Selection and performance-degradation modeling of LiMO2/Li4Ti5O12 and LiFePO4/C battery cells as suitable energy storage systems for grid integration with wind power plants: An example for the primary frequency regulation service. IEEE Trans Sustain Energy Jan. 2014;5(1):90–101.
[21] UK needs at least 50GW of energy storage for net zero by 2050, National Grid ESO says, Future Energy Scenarios: 50GW of energy storage by 2050 for net zero (energy-storage.news).
[22] Mu Y, Wu J, Ekanayake J, Jenkins N, Jia H. "Primary frequency response from electric vehicles in the Great Britain power system. IEEE Trans Smart Grid Jun. 2013;4(2):1142–50.
[23] Moghadam MRV, Zhang R, Ma RT. Distributed frequency control via randomized response of electric vehicles in power grid. IEEE Trans Sustain Energy Nov. 2016;7(1):312–24.
[24] Chen S, Zhang T, Gooi HB, Masiello RD, Katzenstein W. Penetration rate and effectiveness studies of aggregated BESS for frequency regulation. IEEE Trans Smart Grid Jan. 2016;7(1):167–77.
[25] Ghosh S, Kamalasadan S, Senroy N, Enslin J. Doubly fed induction generator (DFIG)-based wind farm control framework for primary frequency and inertial response application. IEEE Trans Power Syst May 2016;31(3):1861–71.
[26] Wu Z, Gao W, Zhang H, Yan S, Wang X. "Coordinated control strategy of battery energy storage system and PMSG-WTG to enhance system frequency regulation capability. *IEEE Trans. Sustain. Energy*. In Press.
[27] Li Y, Xu Z, Wong KP. "Advanced control strategies of PMSG-based wind turbines for system inertia support," *IEEE Trans. Power Syst*. In Press.
[28] Arani MF, Mohamed YA. "Analysis and mitigation of undesirable impacts of implementing frequency support controllers in wind power generation. IEEE Trans Energy Convers Mar. 2016;31(1):174–86.
[29] Lee J, Jang G, Muljadi E, Blaabjerg F, Chen Z, Kang YC. Stable short-term frequency support using adaptive gains for a DFIG-based wind power plant. IEEE Trans Energy Convers Sep. 2016;31(3):1068–79.
[30] Ye H, Pei W, Qi Z. Analytical modeling of inertial and droop responses from a wind farm for short-term frequency regulation in power systems. IEEE Trans Power Syst Sep. 2016;31(5):3414–23.
[31] Wilches-Bernal F, Chow JH, Sanchez-Gasca JJ. A fundamental study of applying wind turbines for power system frequency control. IEEE Trans Power Syst Mar. 2016;31(2):1496–505.
[32] De Almeida RG, Lopes JP. Participation of doubly fed induction wind generators in system frequency regulation. IEEE Trans Power Syst Aug. 2007;22(3):944–50.
[33] Azizipanah-Abarghooee R, Malekpour M, Karimi M, Terzija V. Development of the equivalent Great Britain 36-zone power system for frequency control studies. Int J Electric Power Energy Syst Nov. 2023;153:109390.
[34] GB 36 Bus Electricity Transmission Network DIgSILENT PowerFactory Model, National Grid ESO. [Online]. Available: GB 36 Bus Electricity Transmission Network Model | ESO (nationalgrideso.com).
[35] Demetriou P, Asprou M, Quiros-Tortos J, Kyriakides E. "Dynamic IEEE test systems for transient analysis. IEEE Syst J Jul. 2015.
[36] National Grid, Innovation, Enhanced frequency control capability project, [Online]. Available: https://smarter.energynetworks.org/projects/ngeten03.
[37] Azizipanah-Abarghooee R. Wide-area monitoring based smart frequency control in future low-variable inertia systems with CCGT/wind/PV/BES/load, PhD Thesis, The University of Manchester (United Kingdom); 2019. [Online]. Available: https://www.research.manchester.ac.uk/portal/en/theses/widearea-monitoring-based-smart-frequency-control-in-future-lowvariable-inertia-systems-with-ccgtwindpvbesload(79eb04c3-5b5a-41b2-8d54-b20ecad1cb88).html.
[38] MIGRATE Project, [Online]. Available: https://www.h2020-migrate.eu/.
[39] Clark K, Miller NW, Sanchez-Gasca JJ. Modeling of GE wind turbine-generators for grid studies. GE Energy 2010 Apr;16:4.
[40] Ackermann T. Wind power in power systems, vol. 140. Chichester, UK: John Wiley; 2005.
[41] Kjær SB. "Design and control of an inverter for photovoltaic applications," Ph.D. dissertation, Dept. Energy Technol., Inst. Energy Technol., Aalborg Univ., Aalborg, Denmark, 2005.
[42] Kjær SB. Evaluation of the "Hill Climbing" and the "Incremental Conductance" Maximum Power Point Trackers for Photovoltaic Power Systems. IEEE Trans Energy Convers Dec. 2012;27(4):922–9.
[43] Chahwan J, Abbey C, Joos G. "VRB modelling for the study of output terminal voltages, internal losses and performance." Electrical Power Conference, 2007. EPC 2007. IEEE Canada. IEEE, 2007.
[44] Korpaas M, Holen AT, Hildrum R. Operation and sizing of energy storage for wind power plants in a market system. Int J Electr Power Energy Syst 2003;25(8):599–606.
[45] Yazdani A, Iravani R. Voltage-sourced converters in power systems: Modeling, control, and applications. John Wiley & Sons; 2010.
[46] Arani MFM, Mohamed YARI. Analysis and mitigation of undesirable impacts of implementing frequency support controllers in wind power generation. IEEE Trans Energy Convers March 2016;31(1):174–86.